



## OPEN Comprehensive genomics, probiotic, and antibiofilm potential analysis of *Streptococcus thermophilus* strains isolated from homemade and commercial dahi

Aiswarya Sudheer<sup>1</sup>, Debabrata Ghosh Dastidar<sup>2</sup>, Gourav Ghosh<sup>2</sup>, Zarin Taj<sup>1</sup>, Illathu Kandy Nidhin<sup>1</sup> & Indranil Chattopadhyay<sup>1</sup>✉

This study investigated the probiotic properties and antibiofilm potential of *Streptococcus thermophilus* strains obtained from homemade and commercial dahi. The *S. thermophilus* strain from homemade dahi had greater acid tolerance than the commercial strain, indicating a greater capacity to live in the acidic environments of the stomach. The commercial strain had increased survivability in bile salts and was more hydrophobic than the homemade strain. These findings suggest improved adaptability and increased colonization in the gut. The genomes of both strains included genes associated with probiotic characteristics implying that the two strains may provide unique probiotic advantages. These findings highlight the importance of cell-free supernatants (CFS) of these strains in reducing biofilm formation of pathogenic bacteria. Gas chromatography-mass spectrometry demonstrated that 2, 4-di-tert-butylphenol was a shared metabolite in the CFSs of both strains; however, 2-butanol was found only in the CFS of the homemade dahi strain. In-silico investigations revealed that compounds have drug-like characteristics, suggesting that they could be used for treating biofilm-associated diseases. This study highlights the health advantages of probiotics found in traditional dahi, but it also provides a way to develop natural antibacterial medicines.

**Keywords** Fermented dairy product, Lactic acid bacteria, Probiotic potential, Whole genome sequence, Antibiofilm activity

Fermented foods and drinks include useful microorganisms, particularly lactic acid bacteria (LAB), which have antibacterial and probiotic effects<sup>1</sup>. Dahi, a traditional yogurt made with *Lactobacillus bulgaricus* and *Streptococcus thermophilus*, is a popular local dairy product in Asian nations, including India<sup>2</sup>. Probiotic dahi consumption decreases glucose intolerance, hyperglycemia, hyper-insulinemia, oxidative stress, and dyslipidemia, implying a reduced chance of diabetes<sup>3</sup>. LABs are facultative anaerobes that play a significant role in the production of dairy products such as yogurt. LAB can be homofermentative or heterofermentative, and they have distinct metabolic properties such as an ideal pH range and bile salt tolerance<sup>4</sup>. LABs are important probiotics that can produce a wide range of beneficial substances and play crucial roles in regulating gut biological processes, which aid metabolism. LAB strains include *Lactiplantibacillus plantarum*, *L. fermentum*, *L. rhamnosus*, *Lactococcus lactis*, *S. thermophilus*, *Weissella paramesenteroides*, and *W. cibaria*, which may provide health advantages to the host<sup>5</sup>. Probiotics have a number of benefits for the host, including allergy mitigation, decreased cholesterol levels in serum, anti-inflammatory activity, antitumor and antibacterial properties, and the prevention of gastrointestinal inflammatory disorders<sup>6</sup>. The majority of these bacteria exhibit probiotic characteristics, including acid resistance, hydrophobicity, autoaggregation, coaggregation, and antagonistic activity against pathogenic bacteria<sup>7</sup>. To be effective, a probiotic strain must be able to tolerate, survive, and colonize diverse environments. Probiotic isolates must survive in low pH gastric juice, resist bile salts, and adhere to intestinal epithelial cells<sup>8</sup>. The hydrophobicity of the bacterial cell surface influences bacterial adhesion<sup>9</sup>. LABs should be antibiotic-sensitive, and able to colonize the human digestive tract and exhibit antibacterial activity<sup>10</sup>. *Lactiplantibacillus plantarum*

<sup>1</sup>Department of Biotechnology, School of Life Sciences, Central University of Tamil Nadu, Thiruvavur 610 005, India.

<sup>2</sup>Guru Nanak Institute of Pharmaceutical Science & Technology, 57/F Nilgunj Road, Panihati, Kolkata 700114, India.

✉ email: indranil\_ch@yahoo.com; indranilchattopadhyay2013@gmail.com

YW11, obtained from Tibetan kefir, is resistant to cefoxitin, erythromycin, and metronidazole and prevents the growth of *Listeria monocytogenes*, *Clostridium difficile*, and *Vibrio cholera*<sup>11</sup>. The genome of *L. plantarum* YW11 has been shown to contain glycoside hydrolase and glycosyltransferase families of carbohydrate-active enzymes, which are necessary for considerable probiotic potential and the modulation of immune responses to a range of pathogens<sup>12</sup>. Soy milk and oat milk fermented with *L. plantarum* strains present potential probiotic, antimicrobial, and antioxidant characteristics. These findings can be used to develop milk-free probiotic alternatives, which will benefit individuals who are unable to eat milk and yoghurt owing to food or allergic limitations<sup>13</sup>. The *L. plantarum* 13–3 strain has also been shown to have cyclic lactone autoinducer, terpenes, T3PKS, and RiPP-like gene clusters, indicating its application in food fermentation<sup>14</sup>. The identification of genetic components, notably bacteriocin gene clusters and prophages in the *L. plantarum* 13–3 strain have important practical ramifications across a variety of scientific disciplines<sup>15</sup>. Scientists are interested in the particular composition of LAB-derived cell-free supernatant (CFS) because of its potential benefits for wellness<sup>16</sup>. Probiotics produce a variety of antibacterial substances including bacteriocins, exopolysaccharides (EPSs), hydrogen peroxide, bacteriolytic enzymes, vitamins, numerous organic acids, and secondary metabolites, which prevent enteric pathogens and bacteria from causing food deterioration<sup>17</sup>. EPSs enable probiotic bacteria to persist in the digestive system<sup>18</sup>. Biofilms account for approximately 80% of infections caused by microbes. Biofilms include either homogenous or heterogeneous populations of bacteria, anchored on a matrix of extracellular polymeric substances which slows the passage of antibiotics through the biofilm. Compared with planktonic cells, biofilm cells exhibit antibiotic resistance through alterations in gene expression<sup>19</sup>. Furthermore, the EPS matrix serves as a safe refuge for biofilm cells, as most antibacterial agents are slowed as they pass through it<sup>20</sup>. In recent years, biofilms have emerged as a major concern for public healthcare, as biofilm-associated illnesses may result in significant tolerance to pharmaceuticals<sup>21</sup>. The antibiofilm efficacy of CFS from probiotics is associated with antagonistic substances such as organic acids, hydrogen peroxide, exopolysaccharides, biosurfactants, and bacteriocins<sup>22</sup>. These antagonistic chemicals can directly destroy the bacterial outer membrane, resulting in cell death. Indeed, several antibiofilm agents have no antibacterial activity against planktonic cells<sup>23</sup>. As a result, it is vital to assess the potential impacts of our LAB strains on the development of biofilms at both the planktonic and sessile phases. Dynamic modelling and molecular docking are used to locate interactions between metabolites of LAB and bacterial virulent proteins of interest<sup>24</sup>.

*S. thermophilus* is a major starter for the dairy industry, enabling the development of popular dairy products such as yogurt and cheese. *S. thermophilus* significantly ferments lactose more than it does glucose. Lactose, the primary sugar found in milk, serves as a key carbon and energy source for *S. thermophilus*, which has adapted to this environment<sup>25</sup>. This strain has clustered regularly interspaced short palindromic repeats (CRISPRs)-CRISPR associated (Cas) (CRISPR-Cas) which may enhance competitive advantages in food environments and defend against bacteriophages and parasitic DNA. Genes obtained via horizontal gene transfer (HGT) may be associated the adaptive features and bacteriocin biosynthesis of *S. thermophilus*<sup>25</sup>. *S. thermophilus* modulates metabolic processes related to blood lipids and glucose, breaks down food nucleosides; inhibits their uptake by gastrointestinal epithelial cells, and can be considered a promising probiotic<sup>26</sup>. Analyzing the genomes of probiotic bacteria can reveal their functions and effects, guiding the development of future probiotics through gene mapping that identifies traits linked to beneficial characteristics<sup>27</sup>.

The present study investigated the probiotic potential of *S. thermophilus* using a combination of in vitro and genomic analyses, with an emphasis on its capacity to withstand various stress conditions, interactions with pathogenic bacteria, and metabolic potential. This study used a multimodal strategy that combines classic probiotic screening assays with cutting-edge bioinformatics approaches to evaluate the functional qualities of strains. Key in vitro experiments were performed to assess the strain's susceptibility to acidic conditions (pH), high salt (NaCl), bile salts, and antibiotic resistance. Furthermore, auto- and co-aggregation capacities were assessed to determine their potential for colonisation in the gastrointestinal system, and cell-surface hydrophobicity was examined to better comprehend their adhesion capabilities. In addition, whole genome sequencing (WGS) of the strains was performed to obtain knowledge about their genetic composition and probiotic abilities, highlighting the significance of the use of probioinformatics—an effective combination of genomics and in vitro experimentation—for identifying probiotic bacteria. This combined approach provides a much more extensive comprehension of probiotic strains than traditional approaches alone. This study also evaluated the antibacterial efficacy of *S. thermophilus* by evaluating its CFS against major pathogenic bacteria. Gas chromatography-mass spectrometry (GC/MS) analysis of the secreted compounds in the CFS was performed to evaluate the metabolic potential of *S. thermophilus* isolated from curd. To our knowledge, this is the first study that systematically investigated the probiotic characteristics and genomic features of *S. thermophilus* strains isolated from home made and commercial curd, providing important insights into potential applications of these strains in health and medicine.

## Materials and methods

### Materials

The chemicals used for this study were procured from HiMedia Laboratories Pvt. Ltd., Mumbai, India. *Staphylococcus aureus* MTCC 740, *Klebsiella pneumoniae* MTCC 618, *Pseudomonas aeruginosa* PAO1 (MTCC 2453), and *Acinetobacter baumannii* MTCC 12,890 were collected from the Microbial Type Culture Collection and Gene Bank (MTCC), Chandigarh, India.

### Sample collection and isolation of lactic acid bacteria

Curd samples were collected under aseptic conditions and serially diluted ( $10^{-2}$ – $10^{-6}$  fold) with a phosphate buffer saline (PBS) solution (Himedia, Mumbai, India), thereafter, a 0.1 ml of aliquot was poured on de Man–Rogosa–Sharpe (MRS) medium (Himedia, Mumbai, India). The plates were then incubated at 37 °C for 24–48 h.

Colony morphology; cultural characteristics and Gram staining were performed for individual distinct colonies on MRS agar (Himedia, Mumbai, India) plates. The pure cultures were preserved at  $-80\text{ }^{\circ}\text{C}$  in 50% glycerol for further study<sup>28</sup>.

### Molecular identification

The isolation of genomic DNA was performed from the selected isolate via a HiPurA<sup>®</sup> Bacterial Genomic DNA Purification Kit (Himedia, Mumbai, India) according to the manufacturer's instructions, and the quality of the isolated DNA was determined via agarose gel electrophoresis. PCR amplification of the 16S rDNA gene was performed with the primers 27F (5'-AGAGTTTGATCATGGCTCAG-3') and 1492R (5'-ACGGATACCTTGT TTAGACTT-3'). A single discrete PCR amplicon band of 1500 bp was observed when it was resolved on agarose gel. Impurities were eliminated from the PCR amplicon. The PCR amplicon was sequenced via a Big Dye Terminator v3.1 kit (Applied Biosystems<sup>™</sup>, USA) on an ABI 3730xl Genetic Analyzer with forward and reverse primers. The forward and reverse consensus sequences of the 16 S rDNA gene were generated via aligner software. The 16 S rDNA sequence was compared with that of reference bacteria from the National Centre for Biotechnological Information (NCBI) GenBank, via the nucleotide BLAST algorithms available at <http://www.ncbi.nlm.nih.gov/blast>. Clustal W software program was used for multiple sequence alignment. A distance matrix was generated, and the phylogenetic tree was constructed using the maximum likelihood method based on the Kimura 2-parameter model in MEGA 11<sup>29,30</sup>.

### Evaluation of probiotic properties

#### *Test for resistance to low pH*

Resistance to pH is one of the essential attributes for identifying acid resistance in gastric regions by in-vitro assay. Because food resides in the stomach for at least three to four hours, this duration constraint was selected for the in vitro assay to measure pH tolerance at pH 2, 3, and 7.2 by adjusting the pH with 1 N HCl. The LAB isolates were cultured in MRS broth overnight at  $37\text{ }^{\circ}\text{C}$ . The resulting cultures were centrifuged at 12,000 rpm for 5 min at  $4\text{ }^{\circ}\text{C}$  and the cell pellets were rinsed twice in PBS (pH 7.2). A total of  $10^8$  cells/ml (OD at 600 nm corresponds to 0.2) were reconstituted in PBS with the pH calibrated to 2.0 and 3.0 by applying 1 N HCl and maintained for 2 and 3 h at  $37\text{ }^{\circ}\text{C}$ . As a control, PBS calibrated to pH 7.2 was used. The total viable population was determined by distributing 100  $\mu\text{l}$  of bacterial culture on MRS agar plates after 24 h of exposure at low pH to the original bacterial concentration at  $37\text{ }^{\circ}\text{C}$ , which was adjusted to 100%. The results are expressed as described by Gharbi et al. (2019)<sup>31</sup>.

#### *NaCl tolerance test*

The NaCl sensitivity of the bacterial isolate was evaluated by spreading it on MRS agar plates containing different concentrations of NaCl (0, 1, 2, 3, 4, 5, and 6%) at  $37\text{ }^{\circ}\text{C}$  for 24 h. MRS agar plates without NaCl were used as a control. The effect of the amount of sodium chloride on the degree of bacterial growth inhibition was determined.

#### *Phenol tolerance assay*

Gut bacteria can convert dietary aromatic amino acids into phenols, which may hinder the growth of lactic acid bacteria, making it essential for probiotics to withstand phenol exposure to survive in the intestines. The phenol tolerance of LAB was tested by culturing the bacteria in MRS broth containing 0.5% phenol at  $37\text{ }^{\circ}\text{C}$  for 24 h. The cultures were serially diluted and placed on MRS agar plates. Cell viability (log CFU/ml) was determined using the plate count method<sup>8</sup>.

#### *Temperature tolerance*

Overnight LAB cultures were placed into MRS broth and cultured at temperatures of 15, 45, and  $37\text{ }^{\circ}\text{C}$  for 24 h. Their growth was then evaluated by measuring their turbidity at 600 nm with a spectrophotometer before being placed on MRS agar plates and incubated for 24–48 h at  $37\text{ }^{\circ}\text{C}$ . Cell viability was determined using the plate count method, and the findings are presented as log CFU/ml.

#### *Bile salt tolerance test*

Bile salts, which are detrimental to living cells and are released by the liver before being stored in the gallbladder, and reaching the intestinal tract, require probiotic strains to develop tolerance for survival in the gastrointestinal environment<sup>32</sup>. Bile tolerance was assessed using MRS containing 0.3% and 0.0% Ox-gall, as measured by the OD600nm hourly for 4 hours. The time required to achieve a 0.3 OD at 600nm was tracked. The impact of bile resistance- 'd' was determined as the variation in growth between the control and isolate measured in minutes. According to the procedure, the isolate is considered a bile tolerant strain if the growth delay 'd' between the control and test to reach 0.3 OD600nm is  $\leq 15$  min. Isolates with  $d > 15$  min and  $\leq 40$  min or  $d > 40$  min and  $\leq 60$  min are considered tolerant or poorly tolerant, respectively<sup>33</sup>.

#### *Cell surface hydrophobicity*

One of the most significant properties of probiotic bacteria is their ability to adhesion, which is influenced by their cell surface hydrophobicity that dictates the level of attachment to gastrointestinal epithelial cells<sup>34</sup>. Three ml of bacterial suspension in PBS (pH 7.2–7.4) was then combined with an equal volume of xylene solvent and vortexed vigorously for 3 min. For phase separation, the mixture was incubated at  $37\text{ }^{\circ}\text{C}$  for 2 h under static conditions. The lower aqueous phase was then carefully collected, and the absorbance was measured with a spectrophotometer at 600 nm. The bacterial affinity for hydrocarbons (hydrophobicity) was reported as a

percentage of adhesion according to the formula  $[(A_0 - A)/A_0] \times 100$ , where  $A_0$  and  $A$  are the initial and final optical density respectively<sup>35,36</sup>.

#### *Cellular autoaggregation*

Autoaggregation determines the ability of bacteria to self-recognize surface structures and attach to each other<sup>37</sup>. The bacterial strains were examined for auto-aggregation using the method reported by Zawistowska-Rojek et al., with some changes<sup>38</sup>. The cell pellets were washed with PBS (pH 7.4) two times before being resuspended in 9 ml of PBS solution (pH 7.4). The initial absorbance at 600 nm was corrected to  $0.25 \pm 0.05$  corresponding to approximately  $10^7$ - $10^8$  CFU/mL. The suspension was incubated at 37 °C for 4 h. An aliquot of 0.1 ml obtained from the topmost layer of the suspensions at 4 h was mixed with 0.9 ml of PBS and its  $A_{600}$  was monitored. The percentage of cellular autoaggregation was determined via the formula  $[(A_0 - A_t)/A_0] \times 100$ , where  $A_0$  is the  $A_{600}$  at 0 h and  $A_t$  represents the  $A_{600}$  of the cell suspension at 4 h.

#### *Coaggregation assay*

Coaggregation is an aggregation between genetically diverse bacterial strains in the human gut where probiotics boost the likelihood of bacterial survival. The absorbance at 600 nm was adjusted to  $0.25 \pm 0.05$  to determine the total count of bacteria ( $10^7$ - $10^8$  cfu/mL). Equal amounts of cells (1 mL) from each probiotic and pathogen strain were combined and incubated at 37 °C without agitation. The absorbance of the mixtures was determined at 600 nm at 0 h and 4 h. Coaggregation was determined by using the formula  $[(Amix_0 - Amix_t)/Amix_0] \times 100$  where  $Amix_0$  represents the absorbance of a bacterial mixture at 600 nm at 0 h and  $Amix_t$  represents the absorbance of a bacterial mixture at 600 nm after 4 h of incubation.

#### *Antibiotic sensitivity test*

The Kirby-Bauer disc diffusion test was used to assess antibiotic sensitivity. Three microlitres of overnight cultured LAB were placed on MRS agar plates with an L spreader to form a lawn and dried for 10 minutes. Antibiotic discs were placed on Mueller-Hinton agar (MHA) plates along with the isolate and incubated for 24–48 h at 37°C. The diameters of the inhibition zones were determined, and the strains were identified using the conventional antibiotic disc chart. Standard antibiotic discs were procured from 'HiMedia, Mumbai, India' which include tetracycline (30 µg), chloramphenicol (30 µg), kanamycin (30 µg), rifampicin (5 µg), erythromycin (15 µg), vancomycin (30 µg), and penicillin-G (10 µg).

### **Safety assessment of LAB strains**

#### *Haemolytic activity*

Overnight LAB isolates that were grown in MRS broth were streaked on sheep blood agar base plates containing 5% (v/v) sheep blood and maintained at 37 °C overnight. The blood agar plate was inspected for signs of  $\beta$ -haemolysis (clear zone around the colonies),  $\alpha$ -haemolysis (green-hued zones around colonies) or  $\gamma$ -haemolysis (no zones around the colonies)<sup>8</sup>.

#### *DNase activity*

The overnight cultures of LAB isolates were streaked onto a freshly prepared deoxyribonuclease (DNase) agar medium (DNase Test Agar w/Toluidine blue- M1041- HIMEDIA) to test production of the DNase enzyme. After 48 h of incubation at 37 °C, the plates were examined for DNase activity. Positive DNase activity was evidenced by a pronounced red or clear pinkish zone surrounding the colonies<sup>30</sup>.

#### *DPPH radical-scavenging assay*

100 µl of CFS was combined with 1.9 ml of methanol. Later, 2 ml of 2, 2-diphenyl-1-picrylhydrazyl (DPPH) (6 mg/100 ml of methanol) was added to the CFS. DPPH activity was determined at 517 nm and results are expressed as described by Goel et al. (2020)<sup>1</sup>.

### **Whole genome sequencing and bioinformatics analysis**

DNA was measured using dS DNA HS Dye at the QUBIT 3 Fluorometer and 100ng of intact DNA was enzymatically digested to produce 200–300 bp of DNA fragment. The DNA fragments undergo end repair, which converts the overhangs caused by fragmentation into blunt ends. The 3' to 5' exonuclease activity of the end repair combination eliminates 3' overhangs, whereas polymerase activity results in 5' overhangs. The adenylation of the blunt-ended fragments is performed by adding a single 'A' nucleotide to the 3' ends. Loop adapters were attached to the adenylated segments and digested with the uracil-specific excision reagent (USER) enzyme. The DNA purified by AMPure beads was amplified by 6 cycles of PCR using NEBNext Ultra II Q5 master mix, Illumina universal primer, and sample-specific octamer primers. The enriched PCR products were again purified with AMPure beads and the DNA library was eluted in 15µl of 0.1X TE buffer. The concentration of the DNA library was measured using dS DNA HS Dye at the QUBIT 3 Fluorometer. The size of the DNA library was estimated on an Agilent 2100 Bioanalyzer by injecting 1 µl of the DNA library into an Agilent DNA 7500 chip. Sequencing was performed by using the Illumina NovaSeq6000 (2 × 151 paired ends) platform<sup>1,26,27</sup>. Adapter removal and trimming were performed by Trim Galore ([https://www.bioinformatics.babraham.ac.uk/projects/trim\\_galore/](https://www.bioinformatics.babraham.ac.uk/projects/trim_galore/)). The quality of the reads was evaluated using FASTQC (version 0.12.0) (<https://www.bioinformatics.babraham.ac.uk/projects/fastqc/>), and low-quality reads were eliminated using Trimmomatic (version 0.39) (<http://www.usadellab.org/cms/?page=trimmomatic>). The forward and reverse reads of the raw data were assembled by using Unicycler based on de novo assembly and the resulting files were stored in .fasta format (<https://github.com/rrwick/Unicycler>). MeDuSa was used for reassembly on the basis of alignments against the corresponding reference sequences<sup>39</sup>. The rapid prokaryotic genome annotation (PROKKA) tool (<http://www.vicbioinformatic>

ics.com/software/prokka.shtml) was used to annotate bacterial genomic DNA sequences<sup>40</sup>. Circular mapping of the annotated genome was performed by using CG view (<https://proksee.ca/>). The cluster of orthologous genes (COG) database was used to identify the functions of uncharacterized genes based on their resemblance to known genes. EggNOGmapper (Evolutionary Genealogy of Genes: Non-supervised Orthologous Groups) version 2.0 tool (<http://eggnog-mapper.embl.de/>) from the online EggNOG database (version 5.0) was used for functional classification of proteins into COGs database. The EggNOG database organizes genes into groups on the basis of evolutionary links<sup>41</sup>. ShinyGO 0.77, a web-based tool, was used for analyzing and displaying annotations of gene ontology (GO) (<http://bioinformatics.sdstate.edu/go74/>). The KEGG (Kyoto Encyclopedia of Genes and Genomes) database was used to assign functional information to genes or proteins sequences by comparing the sequences in the KEGG database by using sequence alignment tools such as BLAST. KASS was used to identify the KO IDs, which were subsequently linked to the appropriate functional categories using the KEGG mapper tool (<https://www.genome.jp/kegg/mapper/>). BlastKOALA (version 2.2) was used to assign the Kyoto Encyclopaedia of Genes and Genomes Orthology (KO) and map the predicted genes to the KEGG databases (<https://www.kegg.jp/blastkoala/>). Clustered regularly interspaced palindromic repeats (CRISPR) inside the assembly were evaluated using CRISPRCasFinder 4.2.30<sup>42</sup>. The BAGEL4 web server (<http://bagel4.molgenrug.nl/>) was used to predict the bacteriocin genes in both strains. The IslandViewer 4 server (<https://www.pathogenomics.sfu.ca/islandviewer/>) was applied to identify complete genomic islands of both strains, demonstrating inherited resistance genes. The OriTfinder web based tool (<https://bioinfo-mml.sjtu.edu.cn/oriTfinder/>) was used to determine the origin of gene transfer regions in bacterial mobile genetic elements, whereas the ICEberg2.0 database (<https://bioinfo-mml.sjtu.edu.cn/ICEberg2/index.php>) detected bacterial integrative and conjugative elements. The MOB-suite tool (<https://github.com/phac-nml/mob-suite>) was utilized to identify the contigs of plasmid in bacterial genome.

### Preparation of CFS from *S. thermophilus*

*Streptococcus thermophilus* isolate at a concentration of  $10^8$  CFU/ml was inoculated in 20 ml of MRS (deMan, Rogosa, and Sharpe) broth at 37 °C at shaking incubator for overnight. The overnight bacterial culture was then centrifuged at 8000 g for 20 min at 4 °C. CFS was collected through a sterile syringe with a needle and filtered through polyethersulfone (PES) membrane filter with a pore size of 0.22  $\mu$ m. The CFS was stored at -20 °C for further study<sup>22</sup>. CFSs were diluted with LB broth and added at several percentages (30, 40, 50, 60, 70, 80, 90%) in a final volume of 200  $\mu$ l<sup>43</sup>.

### Effect of CFS on the metabolism of pathogenic bacteria by Triphenyl tetrazolium chloride (TTC) assay

Briefly, 20  $\mu$ L of a reference bacterial strain suspension was introduced into the inside wells of a 96-well polystyrene microtitre plate with various concentrations ranging from 5 to 90% (v/v) of CFS. A total of 50  $\mu$ L of sterile 0.05% TTC solution was added to each well. To promote bacterial growth and biofilm formation, the plates were incubated overnight at 37 °C under static circumstances. The planktonic cells and spent media were removed, and the adhering biomass was washed three times with distilled water on the following day. The metabolized TTC dye (red in the wells) was dissolved in 100  $\mu$ L of methanol, and gently mixed, and the absorbance at 500 nm was measured on a multimode reader (SpectraMax i3x; Molecular Devices; USA)<sup>44</sup>.

### Microscopic image analysis of biofilms

Microscopic evaluation of images was used to assess the extent of biofilm development by pathogenic bacteria in the presence of CFS. To carry out this study, the coverslips were removed after 24 h and stained with 0.4% crystal violet for 30 min. The coverslips were washed, air-dried, and examined under a compound microscope (RXLR-5)<sup>45</sup>.

### Antibiofilm activity of CFS

Briefly, 20  $\mu$ L of a bacterial suspension was introduced into the inside wells of a 96-well polystyrene microtitre plate with various concentrations (v/v) of CFS. To promote bacterial growth and biofilm formation, the plates were incubated overnight at 37 °C under static circumstances. The next day, bacterial growth was measured by measuring the OD600 of each well with a multimode reader (SpectraMax i3x; Molecular Devices; USA). Planktonic cells and exhausted medium were eliminated and the remaining biomass was rinsed three times with distilled water. The biofilm biomass was stained with a 0.1% crystal violet (CV) solution for 20 min before being washed with distilled water to eliminate any unbound dye. Bound CV was dissolved by adding 70% ethanol and the absorbance was measured at 525 nm using a multimode reader (SpectraMax i3x; Molecular Devices; USA). The percentage of biofilm inhibition was measured as described by Rossoni et al. (2018)<sup>46</sup>.

### Biofilm eradication assay

To form biofilms, 20  $\mu$ L of a bacterial suspension in the media of interest (180  $\mu$ L) was added to the interior wells of a 96-well microtitre plate. The plates were incubated for twenty-four hours at 37 °C for biofilm adherence and development. On the subsequent day, the planktonic and unattached cells were removed from each well, and the adherent biofilm was washed three times with sterile PBS pH 7.4. Different concentrations (v/v) of CFS were added to each well and incubated overnight at 37 °C. The next day, bacterial growth was measured by measuring the OD600 of each well with a multimode reader (SpectraMax i3x; Molecular Devices; USA). Planktonic cells and exhausted medium were eliminated and the remaining biomass was rinsed three times with distilled water. The biofilm biomass was stained with a 0.1% crystal violet (CV) solution for 20 min before being washed with distilled water to eliminate any unbound dye. Bound CV was dissolved by adding 70% ethanol and the absorbance was measured at 575 nm. The medium without CFS along with individual test strains was

utilized as the biofilm growth control. The biofilm eradication percentage was measured as  $[(\text{OD (control)} - \text{OD (test)}) / \text{OD (control)}] \times 100$ .

### Extracellular polysaccharide (EPS) measurement assay

The amount of EPS produced has frequently been tested to determine the amount of bacterial biofilm growth on the surface. Pathogenic bacterial cultures were diluted in sterile BHI or LB or nutrient broth to a maximum concentration of  $10^7$  CFU/ml, treated with 50% (v/v) of CFS, and maintained at 37 °C for 24 h under static conditions. The control was treated with MRS broth. Following incubation, planktonic cells were removed from individual tubes, gently washed, and then subjected to the addition of 5 mL of phosphate buffer saline (pH 7.4). Then, each tube was thoroughly agitated, and the biofilm cell suspension was centrifuged at 8000 rpm for 20 min at 4 °C. After centrifugation, the supernatants were extracted individually and the cell pellet was discarded. Cold absolute ethanol was combined with the whole pooled supernatant and incubated for 1 h at -20 °C. After incubation, the mixture was centrifuged at 8000 rpm for 10 min to obtain the pellet. The EPS pellet was dissolved in 1 ml of sterile distilled water and mixed with 1 ml of phenol and 5 ml of sulfuric acid. Following 10-minute incubation at 30 °C, the OD was determined at 490 nm. EPS production (%) was measured as  $(\text{OD treatment} / \text{OD control}) \times 100^{45}$ .

### Chemical compound analysis of CFS from *Streptococcus thermophilus*

To quantify the organic acid by GC-MS, postbiotic samples were esterified using 100% ethanol and 97% sulfuric acid. At first, 1 mL of the supernatant was esterified with 10 mL of 100% ethanol and 15 drops of sulphuric acid (97% v/v) to produce ethyl ester derivatives. The ethylation procedure was carried out at 80 °C for 1 h with constantly mixing at 200 rpm. After cooling, 20 ml of water was mixed to each sample, which was extracted five times with 50 mL of dichloromethane. Sodium sulphate (50 g) was included, agitated at 200 rpm for 10 min, and purified through a 0.45 µm membrane filter. The dichloromethane fraction was then recovered and combined. After removing the solvent with a vacuum evaporator at 50 °C, the residue was mixed in 5 mL of dichloromethane and exposed to gas chromatography measurement (Agilent Model: CH-GCMSMS02, 8890 GC System, 7000 GC/TQ) which is controlled by Agilent GC/MS Mass Hunter Acquisition software. The GC was supplied with an Agilent column (length: 30 m, film thickness: 250 µm, ID: 0.25 µm). Helium was utilized as the carrier gas at a flow rate of 1 mL min<sup>-1</sup>. Experimental parameters of the GC system include the following: Collision Gas: Nitrogen; Temperature program: 50 °C with a 1 min duration; run time: 1 min, 5 °C / min 120 °C hold for 1 min run time 16 mins, 10 °C / min 210 °C hold 1 min, run time 26 min, 10 °C / min 280 °C hold 5 min run time 38 min. Mass spectra were obtained at eight spectra per second ranging from 30 to 900 m/z. The components were detected through matching the corresponding retention times and fragmentation patterns of their mass spectra to those reported in the literature and Wiley Spectral library of the GC/MS instrument. Metabolite set enrichment analysis was performed by MetaboAnalyst 6.0 on the basis of the hypergeometric test. Over Representation Analysis (ORA) was used to examine whether a specific metabolite set is overrepresented by chance in the given compound list. Following adjustment for multiple testing, one-tailed p values ( $P < 0.05$ ) are reported.

Fourier transform infrared (FTIR) spectroscopy was used with an FTIR spectrophotometer (Thermo Scientific™ Nicolet™ iS50 FTIR Spectrometer) to identify functional groups in the CFS of both strains by culturing the cell mass under normal conditions. After 24 h of growth at 37 °C, the cell pellets from each culture were separated using centrifugation. The CFSs were lyophilized for 24 h after rinsing well with 1X PBS buffer solution (pH 7.4). The dry masses were pulverized using an agate mortar and pestle. After powdering, the samples were analyzed using FTIR. A 13 mm die pellet was created by combining 1 mg of each sample with 100 mg of KBr. The samples were scanned 32 times each. The peak adsorptions varied from 400 to 4000 cm<sup>-1</sup> with 4 cm<sup>-1</sup> spectral resolution. OMNIC9.9.549 software was used to analyze the data.

### Pharmacological potential and ADMET parameter analysis of compounds derived from CFS

The Swiss ADME web server (<http://www.swissadme.ch/>) was used to estimate drug ADME parameters (adsorption, distribution, metabolism, and excretion). The structure SMILES was uploaded into the dashboard of the website to evaluate the pharmacokinetic properties of compounds. The toxicity and LD50 of the compounds were evaluated by using ProTox 3.0 (<https://comptox.charite.de/protox3/>). The pharmacological effects of secondary metabolites were assessed using the PASS online server (<https://www.way2drug.com/passonline/>). The obtained data were categorized as probably active or inactive, designated by Pa and Pi, respectively<sup>47,48</sup>.

### Molecular Docking and molecular dynamics (MD) simulations

The target proteins retrieved from the PDB database were processed further for the docking analysis. Non-standard residues, which encompassed residues other than amino acids, were eliminated from the target proteins using the DS client. The resulting protein structures were then subjected to the 'protein preparation wizard' within Maestro, Schrödinger's suite, for further refinement<sup>49</sup>. To prepare the ligand molecules, we acquired their three-dimensional structures from the PubChem database (<https://pubchem.ncbi.nlm.nih.gov>). To make them suitable for docking, we implemented various procedures using the LigPrep v4.7 module of the Schrödinger suite, which encompasses the elimination of salts, addition of H-atoms, and deprotonation. Additionally, to achieve biologically relevant pH (pH 7.0 ± 0.2), the Epik v4.7 module was employed to neutralize the charges of the drug candidates. The virtual screening workflow module of Maestro was then utilized to predict the most suitable drug candidate(s) for different target proteins<sup>50</sup>. We employed the 'receptor grid generation module' to create grids with a size of 20 Å, spanning the entire binding site area. The screening of ligands involved molecular docking using the Glide Virtual Screening Workflow (VSW). Various parameters such as the Glide score, Glide energy, and Glide emodel were recorded. The Discovery Studio Client, specifically version 16.10

(Accelrys Software Inc., San Diego), was utilized for post-docking binding-site analysis and the generation of graphical representations. To determine the binding energies between the ligands and the target proteins, we employed the molecular mechanical-generalized born surface area (MM-GBSA) score calculation. This was carried out using the Prime MMGBSA module within the Schrodinger suite. The binding energy was calculated using the following equation: MM – GBSA ( $\Delta G$  binding) = Energy of Optimized Complex – Energy of Optimized Receptor – Energy of Optimized Ligand<sup>51</sup>. The protein-ligand complex conformation was investigated by doing molecular dynamics simulations using the “Desmond V 7.2 package” (Schrodinger 2020-3), with a focus on the alterations induced by different solvent systems<sup>52</sup>. The OPLS forcefield was employed for the molecular dynamics simulation (MDS) of the docked complex with the highest glide score. The complex was positioned in the middle of a cubic box. TIP3P water molecules and buffers were added to the box, with a space of 10 Å between the box edge and the protein atom, to conduct dynamic simulations. The volume of the boundary condition box was calculated using complex type, and counter ions (Na<sup>+</sup> and Cl<sup>-</sup>) were randomly injected to neutralize the system. The simulation's progress, energy, and atomic coordinates were meticulously documented at regular intervals of 100 picoseconds throughout 100 ns simulation. During visualization and analysis, the total energy, RMSD, RMSE, ligand-protein interactions, and gyration radiation of of top docked-complex systems were evaluated. To analyze the trajectories, the frames were collected and inspected using the simulation interaction diagram tool, which aided in identifying fluctuations.

### Statistical analysis

All of the tests were performed in triplicate. The standard deviation is represented by error bars on the graphs. One-way analysis of variance (ANOVA) was used to examine the data by GraphPad Prism software version 7.0 for Windows (San Diego, CA, USA). The research study groups' averages were compared using a t-test. Differences were considered statistically significant at  $p \leq 0.05$ .

## Results & discussion

### Morphological and molecular characterization of LAB strains obtained from homemade and industrial curd

We isolated eight isolates from homemade and commercial dahi collected from surrounding the region to the campus and local city of Thiruvapur (Tamil Nadu, India). We analyzed colony shapes and utilized them to evaluate their probiotic properties. The present study reports the prevalence of Gram-positive creamy white, circular, spherical to ovoid nonmotile coccus in homemade and industrial curd. The isolated colonies were white colonies on MRS agar plates without pigmentation. All the selected isolates were catalase negative and grew well at 37°C (Fig. S1). The microbial load of lactic acid bacteria in homemade curd was  $1.64 \times 10^8$  CFU/ml whereas the microbial load of lactic acid bacteria in commercial curd was  $3.34 \times 10^8$  CFU/ml. The 16 S rDNA sequence of the isolated bacteria was utilized to determine their degree of similarity to the existing database sequence. On the basis of these data, both isolates were identified as *Streptococcus thermophilus*. The isolated strain was aligned with *Streptococcus thermophilus* ATCC 19,258 16 S ribosomal RNA, partial sequence NR\_042778.1. Table S1 displays the NCBI GenBank accession numbers for all the isolates with a homology of more than 98% (Table S1).

### Comparison of the probiotic potential of *Streptococcus thermophilus* strains obtained from homemade and commercial Dahi

The digestion of food can take up to 3 h in the stomach ecosystem (pH 2) and 3–8 h in the intestine (pH 8), which are harsh circumstances. To guarantee that a medicine survives these conditions, it must be resistant to bile and gastrointestinal juices, which include many enzymes that would normally destroy the molecules, making them inert<sup>10</sup>. Sensitivity to low pH (2–3) is essential for bacteria to survive in the stomach for 2–3 h during food transit, making them suitable for probiotic use<sup>53</sup>. *S. thermophilus* Sample2B showed a survival of 6.07 log CFU/mL at pH 2 for 4 h and 7.61 log CFU/mL at pH 3 for 4 h. *S. thermophilus* AARV showed a survival rate of 5 log CFU/mL at pH 2 for 4 h and 5.77 log CFU/mL at pH 3 for 4 h. *S. thermophilus* Sample 2B presented high acid tolerance compared with *S. thermophilus* AARV strain. Reducing the pH from 3 to 2 decreases the survival of cells. At both pH 2 and pH 3 for both time points (4 h and 2 h), there were significant differences in growth between both strains of *S. thermophilus* ( $P < 0.05$ ). Both strains had high survival rates when exposed to pH 3. *S. thermophilus* Sample 2B strain showed the maximum acid tolerance (survival rates of 93% and 91% at pH 3 after 2 and 4-h of exposure), followed by the *S. thermophilus* AARV strain (survival rates of 76.84% and 68.35% at pH 3 after 2 and 4-h of exposure, respectively). Both strains presented a reduction in the survival rate at pH 2 after 2 and 4 h of exposure (Table 1). Probiotic bacteria found in dairy and fermented products have been shown to tolerate low pH<sup>6</sup>. Probiotic isolates of *Lactobacillus* and *Bifidobacterium* were less likely to survive in gastrointestinal tract fluids after dietary preservation. Adding *Bacillus* bacteria with probiotic qualities to a food matrix did not result in a decline, with survival rates over 80% even at the end of shelf life<sup>54</sup>. Slower metabolism in the gastrointestinal tract results in decreased probiotic content. Furthermore, the pH of the stomach fluctuates during the day depending on the food consumed; therefore combining probiotics with foods and liquids with a relatively higher pH may be beneficial<sup>55</sup>. *S. thermophilus* from Sample 2 showed acid resistance due to F<sub>1</sub>Fo-ATPase activity. The F<sub>1</sub>Fo-ATPase complex, driven by ATP hydrolysis, regulates the intracellular pH and solute transport, and its efficiency enhances with decreasing extracellular pH in these bacteria<sup>7</sup>. *S. thermophilus* Sample 2B strain could withstand salinities up to 6% NaCl (w/v) whereas *S. thermophilus* AARV strain was capable of withstand salinities of up to 3% NaCl (w/v) (Table 1). Isolates that sustain gastric juice environments were tested for phenol resistance, revealing different levels of sensitivity as phenol is a toxic bacteriostatic chemical generated by gut bacteria during the deamination of aromatic amino acids<sup>56</sup>. Both *S. thermophilus* strains were less tolerant to 0.5% phenol (Table 1). For a microbe to qualify as a prospective probiotic it must be capable of inhibiting pathogen growth and tolerating harmful compounds such as phenol released during certain digestive processes

Strains		Streptococcus thermophilus (SAMPLE 2B)	Streptococcus thermophilus (AARV)
Hydrophobicity with xylene (%)*		51.47 ± 1.03	86.41 ± 2.61
Autoaggregation at 4 h (%)		92.03 ± 2.66	91.46 ± 1.82
Haemolytic activity		Gamma (Υ)	Gamma (Υ)
DNase activity		Negative	Negative
DPPH radical scavenging activity (%)		33.79 ± 0.28	31.16 ± 0.66
pH tolerance*	Control	Time point	Log 10 CFU/mL (survival %)
		T2	8.07 ± 0.03(100)
	T4	8.2 ± 0.02(100)	
	pH 2	T2	4.94 ± 0.03(61.19 ± 0.51)
		T4	6.05 ± 0.03(73.72 ± 0.13)
	pH 3	T2	7.51 ± 0.03(93.12 ± 0.66)
T4		7.48 ± 0.01(91.22 ± 0.34)	
Percentage		Log 10 CFU/mL (survival %)	Log 10 CFU/mL (survival %)
NaCl tolerance*	0%- Control	8.49 ± 0.02 (100)	8.5 ± 0.03 (100)
	1%	8.33 ± 0.02 (98.11 ± 0.35)	8.34 ± 0.02 (98.18 ± 0.52)
	2%	8.25 ± 0.04 (97.17 ± 0.58)	8.25 ± 0.02 (97.06 ± 0.46)
	3%	8.13 ± 0.02 (95.82 ± 0.41)	7.08 ± 0.29 (83.28 ± 3.11)
	4%	7.04 ± 0.03 (82.91 ± 0.44)	4.61 ± 0.12 (54.21 ± 1.51)
	5%	6.67 ± 0.11 ± (78.61 ± 1.44)	1.95 ± 0.1 (22.89 ± 1.05)
	6%	5.58 ± 0.04 (65.76 ± 0.59)	1.5 ± 0.2 (17.67 ± 2.41)
Phenol tolerance*	Control (0%)	8.49 ± 0.02 (100)	8.5 ± 0.03 (100)
	0.5%	2.17 ± 0.22 (25.52 ± 2.58)	2.88 ± 0.08 (33.84 ± 0.78)
Temperature tolerance*	37 °C Control	8.49 ± 0.02 (100)	8.5 ± 0.03 (100)
	45 °C	6.91 ± 0.03 (81.44 ± 0.21)	8.15 ± 0.13 (95.88 ± 1.19)
	15 °C	1.99 ± 0.05(23.51 ± 0.57)	4.87 ± 0.03 (57.33 ± 0.18)

**Table 1.** Comparison of probiotic properties of *Streptococcus thermophilus* strains obtained from homemade and industrial curd. \*P-values < 0.05 indicate statistical significance across all comparisons as compared to control.

in the digestive tract<sup>57</sup>. *S. thermophilus* strains of Sample 2B and AARV were grown at 45 °C. Both strains were tolerant to high temperatures, i.e., 45 °C. At 15 °C, the survival of the Sample 2B strain was lower than that of the AARV strain (Table 1). Bacteria depend considerably on temperature to survive and grow. Bacteria may develop more slowly at high or low temperatures. Dairy manufacturing and processing often involve freeze-drying and heat treatments. Therefore, a probiotic should be temperature-tolerant<sup>4</sup>.

Bile salts are the primary constituents of human gastrointestinal juice. Bile salt tolerance improves colonization in the gastrointestinal tract. Evaluating the development of probiotics in environments containing bile salt is important. The natural levels of human bile range from 0.1% (v/v) to 0.5%, with 0.3% bile salt level deemed crucial for choosing resistant bacteria<sup>58</sup>. Bile salt tolerance is a basic prerequisite for gastrointestinal bacterial survival and colonization, making it one of the most important features of probiotic bacteria<sup>59</sup>. The percentage of persistent LAB bacteria was evaluated after exposure to 0.3% bile salt for four hours. *S. thermophilus* strain's growth in MRS with 0.3%, and 0.0% ox-bile was measured hourly for 4 h using OD 600 nm. The duration required to achieve a 0.3 OD600nm was tracked. The impact of bile suppression ('d') was measured as the difference in growth between the control and isolate in minutes. *S. thermophilus* strains AARV and Sample 2B showed significantly different tolerances to 0.3% bile media. *S. thermophilus* strain AARV exhibited greater survival in 0.3% (w/v) bile salt medium as compared to *S. thermophilus* strain Sample 2B (Fig. 1). Tolerance could be attributed to the presence of functional bile acid/salt efflux pumps, bile salt hydrolysis, and modifications in the makeup of the cell membrane and cell wall<sup>56</sup>. In the study, the different levels of resistance to bile salt of the isolates may depend on the expression of bile resistance-associated proteins in the LAB cells<sup>60</sup>.

For a bacterial cell to adhere to the gastrointestinal system, the cell membrane must contact the host cell surface, making examination of the hydrophobic nature of the cell surface crucial for successful colonization<sup>61</sup>. The hydrophobic characteristics of the outer cell membrane in LABs influence their surface hydrophobicity, which is crucial for assessing how well these strains adhere to and colonize epithelial cells<sup>10</sup>. Xylene was utilized to determine the hydrophobicity of the cell surface. The cell surface hydrophobicities for *S. thermophilus* from both types of curd for the hydrocarbon xylene (non-polar solvent) were 51.47392 ± 1.030187% and 86.39821 ± 2.607392% respectively. *S. thermophilus* AARV strain from commercial dahi was more hydrophobic than was isolated from homemade dahi (Table 1). Autoaggregation promotes the colonization of probiotic bacteria in the intestine and considerably adheres to the intestinal epithelium, reducing pathogen adherence. Bacteria can autoaggregate in three ways: high (50% and above), medium (35–50%), and low (16–35%)<sup>62</sup>. Autoaggregation of *S. thermophilus* from both types of curd was found to be 91.438 ± 2.92% and 92.191 ± 3.61%, indicating their ability to serve as potential probiotics and colonize the intestinal epithelium to some extent.

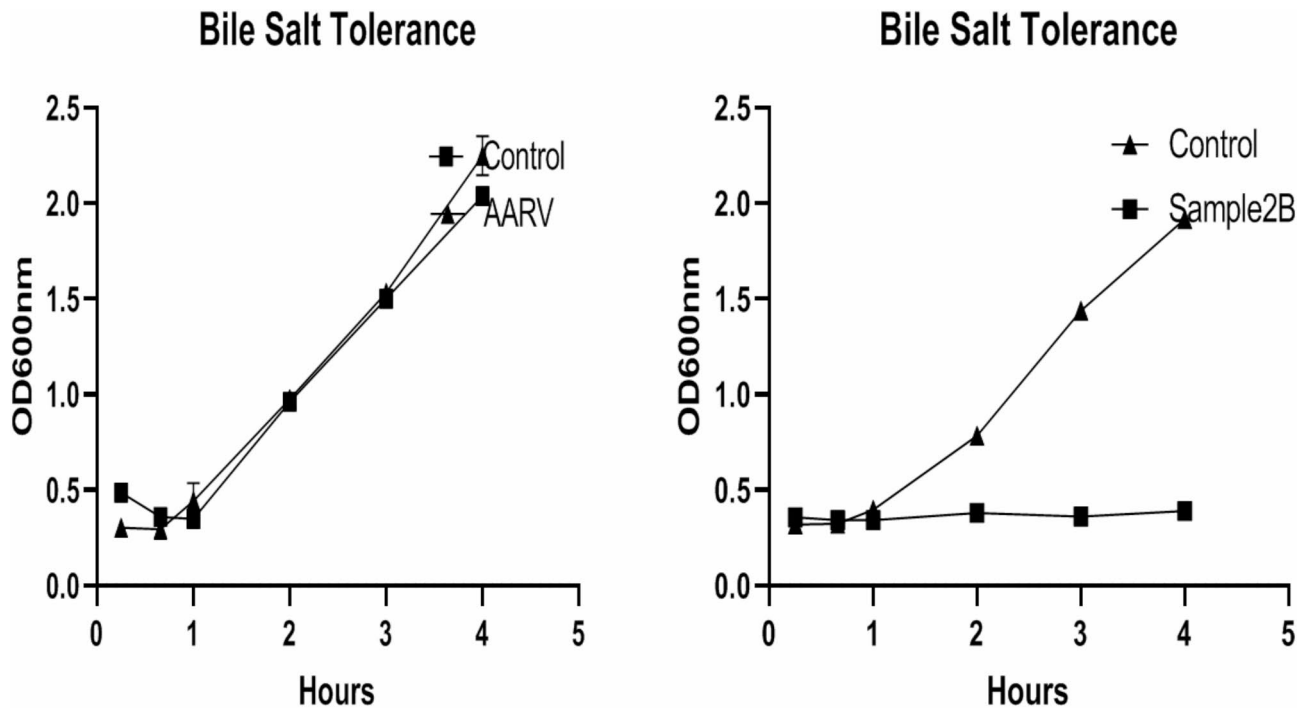


**Fig. 1.** Tolerance of *Streptococcus thermophilus* AARV and Sample2B strain to bile salts 0.3% w/v as compared to control 0.0%.

This study revealed that the degree of autoaggregation was greater than 80% (Table 1). This event aids in the preservation of an ecologically balanced environment in the gut. The capacity to coaggregate varies for each pathogenic strain. The highest degree of coaggregation was observed between *S. thermophilus* from both types of curd and *Staphylococcus aureus* whereas the lowest coaggregation was reported in tests conducted with *Pseudomonas aeruginosa* (Table S2). *S. thermophilus* isolated in this study can autoaggregate and coaggregate pathogens, which could be beneficial for gut health.

Both *S. thermophilus* strains were sensitive to erythromycin, tetracycline, and chloramphenicol. However, the strains were resistant to kanamycin (Table S3). Probiotics may acquire resistance to antibiotics because of their genetic makeup<sup>63</sup>. Antibiotic resistance in beneficial bacteria may allow antibiotics to survive in the intestinal tract. Probiotics with endogenous resistance can improve the gut flora during antibiotic therapy. Probiotic strains resistant to certain antibiotics can improve intestinal microbiome recovery during antibiotic therapy. Antibiotic resistance is a crucial element for assessing the safety of LAB<sup>60</sup>.

*S. thermophilus* strains showed no signs of haemolysis when grown on blood agar for 24 h under anaerobic conditions. The lack of haemolytic activity is a requirement for screening probiotic strains, ensuring that these bacteria are not pathogenic and are harmless to human intake. *S. thermophilus* isolated from both types of curd have been reported to be  $\gamma$  hemolytic (Table 1). Probiotic strains with low hemolytic activity are safer to use because of their non-virulent nature and lack of hemolysin, which prevents virulence among bacteria. The absence of a hemolysis zone surrounding the bacterial colonies indicates the safety of microbe<sup>48</sup>. The DNase test was also used to determine the infectious potential of bacteria which generate DNase enzyme that breaks down DNA by hydrolyzing the phosphodiester bond in the backbone. As a result, the absence of DNase in the tested isolates was established, confirming the possible safety of their utilization in fermentation. The assay findings revealed that none of the isolates had pathogenic factors (Table 1). Table 1 shows the antioxidant capacity of the two isolates. Both isolates demonstrated good antioxidant capacity. LAB extracts can chelate metal ions, scavenge reactive oxygen species, and reduce activities, potentially leading to a lower redox potential in the gut because of their ability to neutralize free radicals<sup>31</sup>. The hydroxyl radical scavenging action of LAB isolates is attributed to the invasion and multiplication of viable cells in the gut<sup>8</sup>. Probiotic colonisation in the gut helps to create an anti-inflammatory environment and reduces the synthesis of important pro-inflammatory cytokines<sup>64</sup>.

### Comparative genomic analysis of both *S. thermophilus* strains

Whole-genome sequencing and comprehensive bioinformatic analysis were used to investigate the genomic properties of *S. thermophilus*, resulting in the building of its genome map. The outermost circle represents the location coordinates of the genomic sequence. Circles display the following characteristics from the outside circle to the center that indicate coding genes, and GC content. GC skew and the GC content play an important role in comprehending the genomic structure. GC skew may anticipate transcriptional orientation and recognize coding strands in bacterial genomes (Fig. 2A, B). Bacteria with high GC contents may require more energy during replication, which has been linked to genome stability. The outside of the circle represents the genomic sequence's location parameters. The complete genome of *S. thermophilus* AARV strain has a length of 1,781,062 bp with a

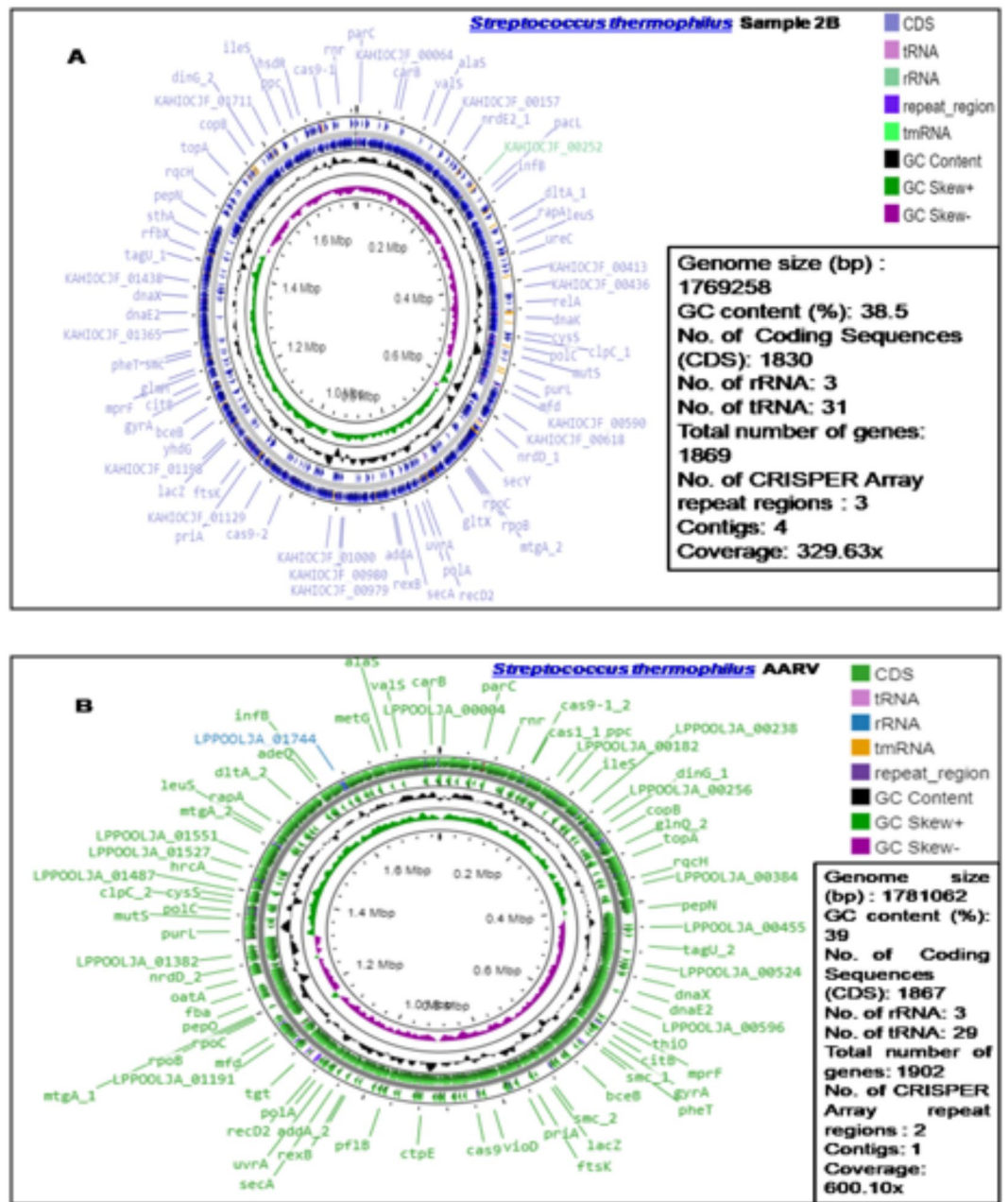


**Fig. 2.** Circular genome map of *Streptococcus thermophilus* Sample 2B (A) and AARV strain (B). Genomic features marked from the outer to the inner circle include CDS (coding sequences), tRNA, rRNA, tmRNA, and repeat region; GC content, GC skew, and genome size. Rapid annotations using subsystems technology (RAST) analysis-based complete subsystem category distribution of whole genome sequence of *S. thermophilus* strains AARV (C) and Sample 2B (D). Each colour in the pie graph indicates biological function with a group of genes mentioned in the right location of the graph. EggNOG category distribution of functional annotation of *S. thermophilus* strains AARV (E) and Sample 2B (F). (G) Comparison of the number of genes assigned to the most prevalent KEGG functional classifications of *S. thermophilus* strains Sample 2B (Blue bars) and AARV (Red bars).

GC content of 39%. Among the 1902 predicted genes, 1867 were found to be protein-coding sequences (CDS) in AARV strain. In addition, 3 rRNAs, 29 tRNAs, and 2 clustered regularly interspaced short palindromic repeats (CRISPR) arrays were identified in AARV strain. The complete genome of the *S. thermophilus* Sample 2B strain has a length of 1,76,9258 bp with a GC content of 38.5%. Interestingly, the GC level was in the same range as that of the previously mentioned *S. thermophilus* strains. Among the 1869 predicted genes, 1830 were found to be protein-coding sequences (CDS) in Sample 2B strain. Furthermore, 3 rRNAs, 31 tRNA, and 3 clustered regularly interspaced short palindromic repeats (CRISPR) arrays were identified in Sample 2B strain. The genome coverage of *S. thermophilus* Sample 2B was 329.63x whereas the genome coverage of the *S. thermophilus* AARV strain was

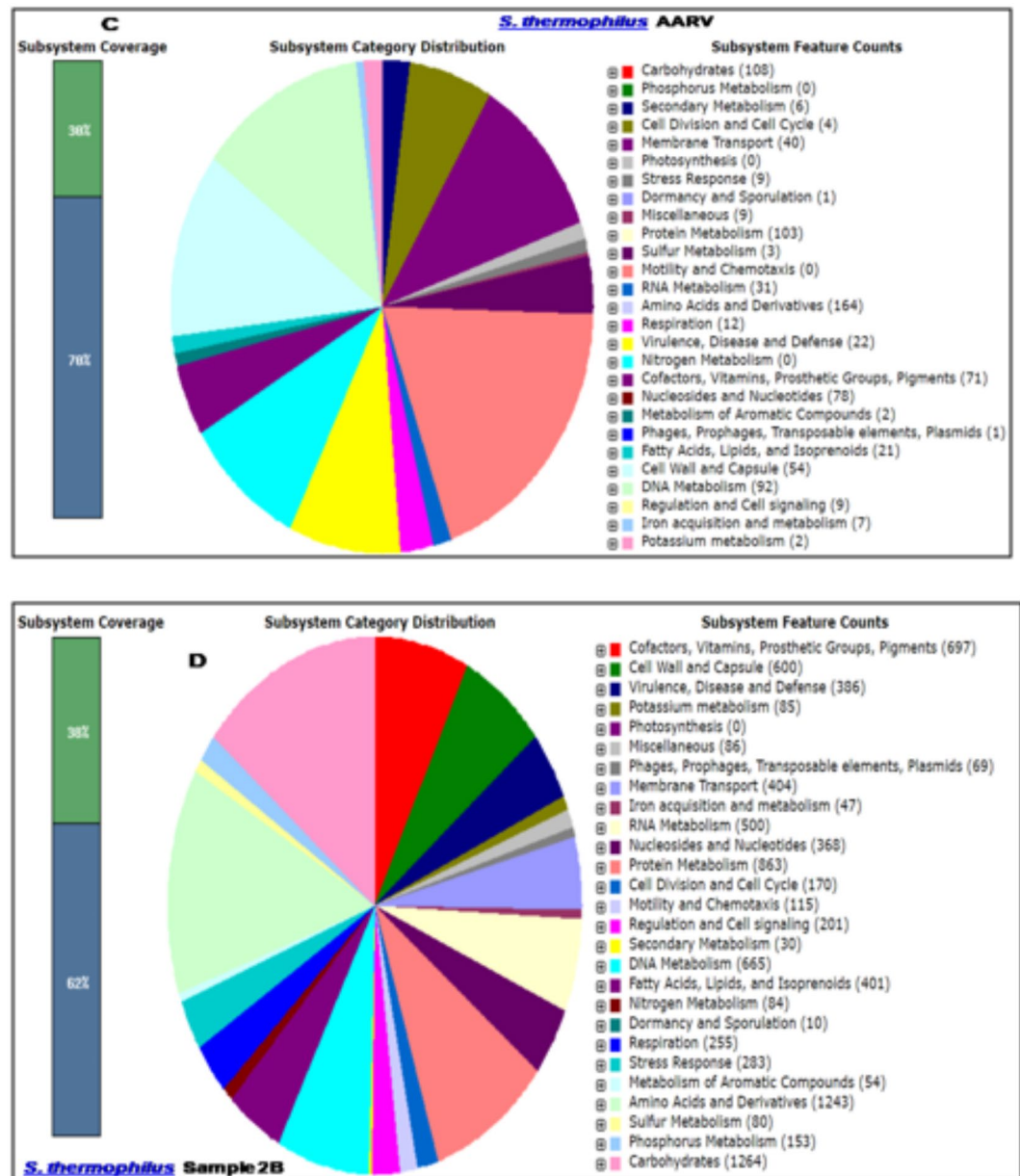
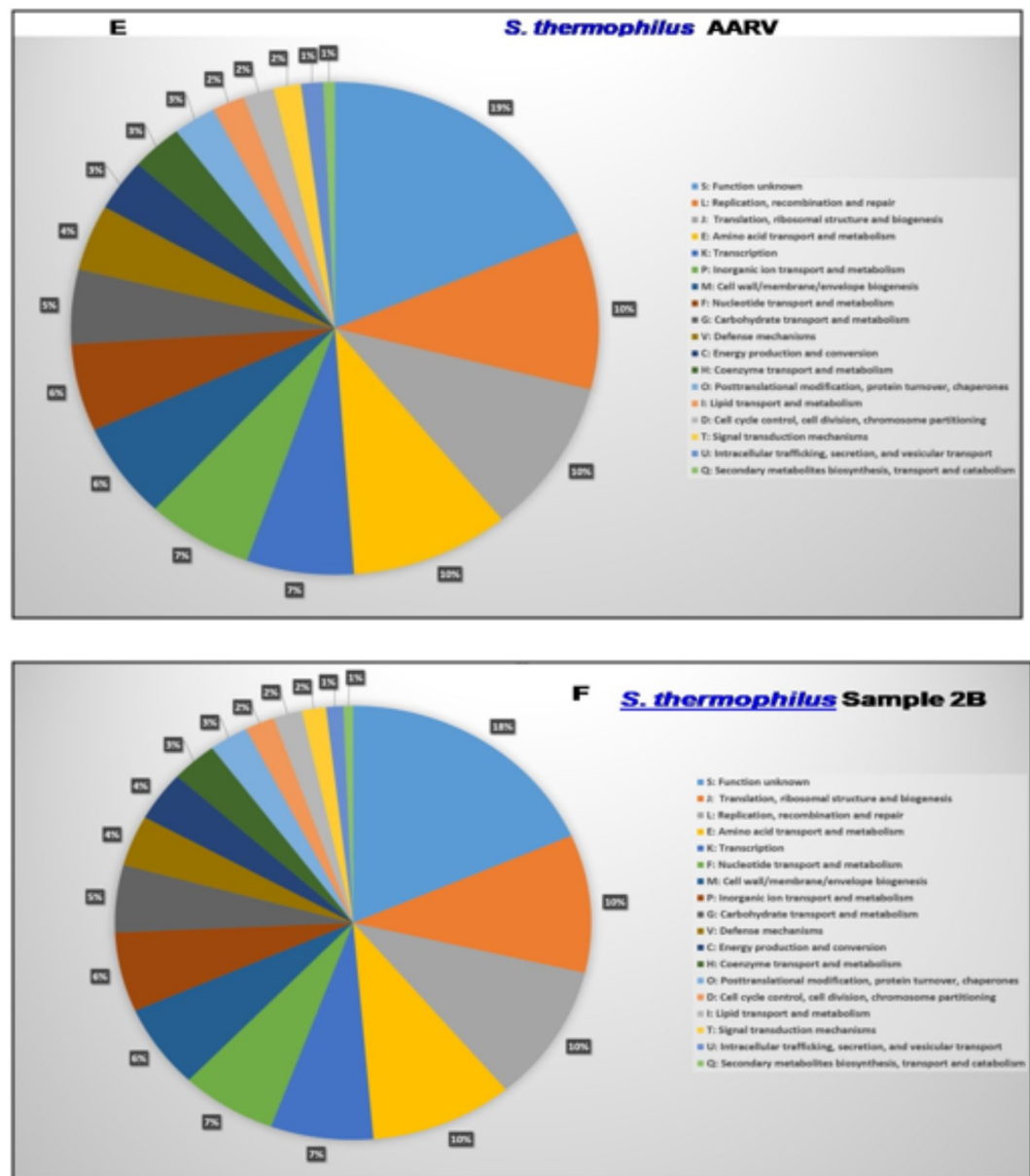


Figure 2. (continued)

600.10x because more reads were generated during sequencing (Fig. 2A, B). Heatmap created from OrthoANI values derived using the OAT (Orthologous Average Nucleotide Identity Tool) programme for isolated *S. thermophilus* and various reference strains. The average nucleotide identity (ANI) is a measure of genomic similarity at the nucleotide level between two genomes' coding regions. The OrthoANI<sub>u</sub> value revealed that both strains shared maximum sequence similarity with the *S. thermophilus* strain EU01. *S. thermophilus* strain EU01 (NZ\_CP047191.1) has a length of 1,948,689 bp with a GC content of 38.8%. Among the 2016 predicted genes, 1927 were found to be protein-coding sequences (CDS) in *S. thermophilus* strain EU01. In addition, 18 rRNAs, 67 tRNA, and 3 clustered regularly interspaced short palindromic repeats (CRISPR) arrays were reported in strain EU01. Strains Sample 2B and AARV were found to display 99% similarity with *S. thermophilus* EU01 (Fig. S2). Many strains of *S. thermophilus* isolated from fermented milk and yogurt have already been sequenced including PNGR-Z-K3, CS5, CS18, CS9, and TSGB4237 whose average genome size is 1.9 Mb with a GC content of 39.5% (Table S4). The results of molecular phylogenetic investigation of two isolates recovered from industrial and traditional curd samples were compared with those of 15 reference strains using 16 S rRNA region. MEGA 11 represents a neighbor-joining and maximum likelihood bootstrap phylogenetic tree with *Limosilactobacillus fermentum* as the out-group. The optimal tree has a branch length of 1.39. The percentages of duplicate trees with clustered associated taxa from the bootstrap test (1,000 repetitions) are presented next to the branches. MEGA 11 was employed to create a phylogenetic tree with additional reference strains from other locations. The results were consistent and confirmed that the strains belong to the same *S. thermophilus*. Sample



**Figure 2.** (continued)

2B strain shows a high proximity with *S. thermophilus* CP017064, whereas AARV strain is far from it in the neighbor-joining phylogenetic tree (Fig. S3). Long-term evolution may have played a role in distinguishing the AARV strain from other strains. The phylogenetic rebuilding of strains on basis of sequenced genomes did not align with their distribution across the globe. Different strains from various regions may cluster together on the same branch, whereas strains from the same country may not be on the same branch<sup>55</sup>. Horizontal gene transfer (HGT) can enhance the technical features of *S. thermophilus* strains by gaining new genes through evolutionary and adaptive changes in the environment. *S. thermophilus* strains exhibit several HGT events, resulting in unique traits and adaptability to various environments. Genes involved in cell replication may enhance strain survival during evolution over time in response to stresses from the environment<sup>65</sup>.

CRISPR is a family of DNA repeats that are distinguished by short, highly conserved regions that are frequently found next to Cas genes. When coupled with Cas proteins, these repeats form the CRISPR-Cas system<sup>66</sup>. The genomes of both *S. thermophilus* strains contain a CRISPR with associated spacer and Cas genes. CRISPRCasFinder identified CRISPR-Cas systems in AARV including CAS-TypeIIU, CAS-TypeIIIA, and CAS-TypeIIA whereas CAS-TypeIIA and CAS-TypeIIU were identified in the Sample 2B strain (Table S5). No phages are detected in either strain. CRISPR-Cas systems, which are found in prokaryotes, confer acquired protection against foreign genetic components such as viruses and plasmids<sup>25</sup>. The Comprehensive Antibiotic Resistance Database (CARD) search by using parameter loose hits and protein homolog model with an identity > 60% was used to identify antibiotic resistance genes in the 2B and AARV strains respectively. The loose hits included

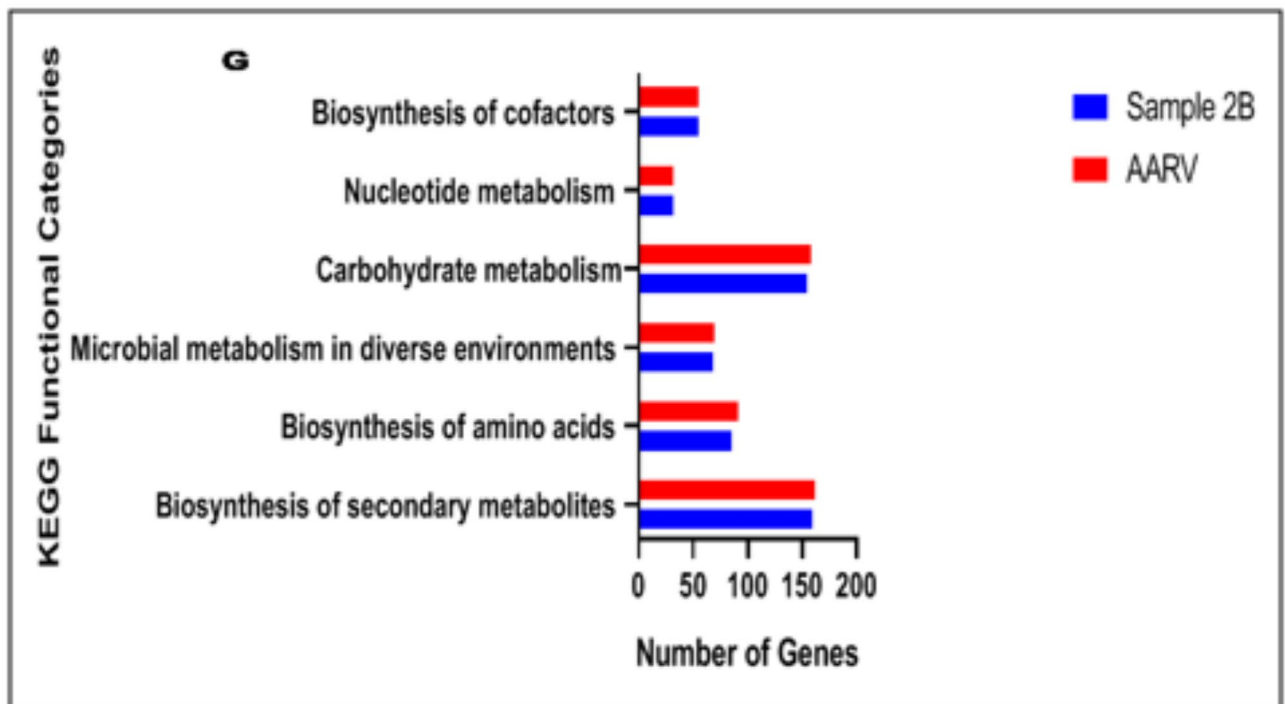


Figure 2. (continued)

genes involved in resistance mechanisms to antibiotic target alterations (antibiotic resistant *fusA* and *elfamycin* resistant *EF-Tu*) and antibiotic efflux (*mreA*) in both strains. The perfect and strict hit criteria identified glycopeptide resistance gene clusters such as the *vanY* gene in *vanB* cluster and the *vanT* gene in *vanG* cluster in both strains (Table S6). Although many probiotics are deemed safe, strains with known resistance mechanisms should be constantly tracked, particularly when used in immunocompromised people or in environments that require frequent antibiotic consumption (e.g., clinics). Inherited antibiotic resistance genes are usually located in mobile genetic elements such as plasmids, transposons, and phages, making them highly transmissible. Bacteriophages can also promote the transmission of genes among bacteria<sup>65,66</sup>. Genomic islands often harbour genes that confer adaptive advantages, such as antimicrobial resistance (AMR), virulence factors, or metabolic capabilities that enhance survival in specific niches<sup>65</sup>. The integrated prediction approach was used to identify many putative genomic islands (GIs) distributed throughout the genome, indicating likely acquisition via HGT. GIs located on these two genomes were identified by the Island Viewer4 software (Fig. S4). It was found that AARV and Sample 2B contained 27 and 16 integrated GIs. The integrated GIs of these two strains harboured 333 and 166 genes, respectively. However, a comprehensive annotation analysis of these regions revealed an absence of homologous virulence-associated genes, AMR determinants, or pathogen-associated loci. This indicates that despite the presence of predicted genomic islands, the strain does not exhibit genomic features typically associated with pathogenicity or antimicrobial resistance. The lack of 'origin of transfer' (*oriT*) regions in the *S. thermophilus* genome indicates a restricted capacity for conjugative gene transfer. The ICEberg2.0 server found no integrative and mobile elements (IME) in the genome of both strains (data not shown). Our investigation of the MOB-suite tool revealed no evidence of plasmid integration into the genome of both strains (data not shown). This is particularly significant, as it implies that the isolated strain is unlikely to facilitate the horizontal transfer of genetic material, even among other *S. thermophilus* strains. Despite the identification of AMR genes in WGS analysis via the CARD database, their lack within projected genomic islands indicates they are not obtained through recent HGT events. This finding is particularly relevant from a food safety perspective, as the HGT of AMR genes inside food-borne microorganisms may contribute to the dissemination of resistance to human pathogens.

The rapid annotations using subsystems technology (RAST) annotation have distributed genes into subsystems. The figure illustrates the subsystems of the *S. thermophilus* strain genome depending on the RAST annotation server. The most abundant genes annotated were associated with amino acids synthesis and their derivatives (164 genes) followed by protein metabolism (103 genes) and nucleoside metabolism (78 genes) in *S. thermophilus* AARV strain isolated from industrial curd whereas in *S. thermophilus* Sample 2B strain, the most prevalent genes identified were related to carbohydrate metabolism (1264 genes) followed by amino acid synthesis and their derivatives (1243 genes), and cofactors, vitamins, prosthetic groups, and pigments (697) (Fig. 2C, D). The COG database is useful for evaluating the functional properties of newly sequenced genomes as well as contrasting microbial communities. KEGG analysis was used to examine the diversity and function of proteins. Genes were first annotated using the KEGG protein ID, then mapped to the KEGG orthology (KO) entry, and finally to the pathway<sup>42</sup>. We conducted an extensive investigation and comparison of COG and KEGG

profiles for the *S. thermophilus* strain. On the basis of COG function grouping, we identified 21 functional categories. The majority of genes in the *S. thermophilus* genome were classified for ribosomal structure and biogenesis (J, 200), amino acid transport and metabolism (E, 175), replication, recombination, and repair (L, 95), and cell wall/membrane/envelope biogenesis (M, 95). EggNOG was used for improving annotation on the basis of Prokka's protein sequence predictions. More than 18% of the proteins had an unknown function (283 proteins), whereas 10% (158 proteins) were involved in translation, ribosomal structure, and biogenesis in the Sample 2B strain of *S. thermophilus*. However, 19% of the proteins had an unknown function (289 proteins), while 10% (157 proteins) are involved in the translation, ribosomal structure, and biogenesis in the AARV strain of *S. thermophilus* (Fig. 2E, F). The highest number of proteins with unknown function indicates the strain's distinctiveness and undiscovered potential. KEGG pathway analysis revealed that a total of 815 genes were participated in 11 KEGG pathways in the Sample2B strain. KEGG pathway analysis of the Sample2B strain suggested that the highest numbers of genes encoding proteins are responsible for the biosynthesis of secondary metabolites (159), microbial metabolism in diverse environments (68), and the biosynthesis of amino acids (85), carbohydrate metabolism (154), nucleotide metabolism (92), and biosynthesis of cofactors (55). However, KEGG pathway analysis of the AARV strain suggested that the highest numbers of genes encoding proteins are responsible biosynthesis of the secondary metabolites (162), microbial metabolism in diverse environments (69), the biosynthesis of amino acids (91), carbohydrate metabolism (158), nucleotide metabolism (31), and the biosynthesis of cofactors (55) (Fig. 2G). The genes were involved in the biosynthesis of cofactors, suggesting the ability of both strains to synthesize vitamins. Pathways associated with central carbohydrate metabolism in the 2B strain included glycolysis and gluconeogenesis (23 genes), pyruvate metabolism (21 genes), amino sugar and nucleotide sugar metabolism (20 genes), the pentose phosphate pathway (11 genes), and starch and sucrose metabolism (16 genes). Furthermore, the full pathways associated with pantothenate biosynthesis (12 genes) and folate biosynthesis (11 genes) were also detected. A similar observation has been reported in the AARV strain.

Genome mining of both *S. thermophilus* strains with Prokka annotation identified 904 genes which are common to both strains whereas 132 genes are unique to the AARV strain and 118 genes are unique to Sample 2B. STITCH network analysis was used to investigate protein-protein interactions and functional interactive networks composed of 14 specifically targeted probiotic proteins such as lacZ, lacS, galT, galK, pflA, trxB1, ackA, galE2, sodA, fola, gor, and dpr etc. (Fig. S5). Common genes are involved in stress resistance (*dnaK*, *hflX*, *gla*, and *gshAB*), sugar metabolism (*nagB*, *glmM*, *glmU*, *glmS*, *manX*, *gtfA*, *rfbC\_1*, *rmlD*, and *glgP*), and adhesion (*cap8A*, *brpA*). Both strains harbor genes encoding enzymes predicted to participate in N-acetylglucosamine catabolism and synthesis (*nagB*) as well as genes responsible for rhamnose biosynthesis (*rmlD\_1*, and *rmlD\_2*). Gene prediction with Prokka revealed the single-copy genes *brpA* and *tagU*, which encode biofilm regulating protein A and polyisoprenyl-teichoic acid-peptidoglycan teichoic acid transferase TagU. Gene prediction of both strains identified *hslO*, which encodes a 33-kDa chaperonin associated with oxidative stress defence. This protein is from the Hsp33 family of molecular chaperones. Two specific genes (*pbpA* and *pbpX*) encoding for penicillin binding proteins and two genes (*rrj1* and *rrj2*) responsible for the resistance to toxic compounds and beta-lactam antibiotics were found in the genome of both the Sample 2B and AARV strains. Other genes such as *dnaK*, *lepA*, *prmA*, *rsmA*, *rsmB*, *rsmC*, *rsmD*, *rsmE*, *rsmF*, *rsmG*, and *rsmH* help safeguard ribosomal function against heat shock and other challenges. Both strains contain *hflX*, which is linked with the 50 S ribosomal subunit and may play a role in the synthesis of proteins and ribosome synthesis. Both strains have genes such as *PflA*, *gadB*, and *gadC* which encode pyruvate-formate lyase activating enzyme, glutamate decarboxylase enzyme, and GABA/Glutamate antiporter respectively (Table S7). *S. thermophilus* Sample 2B strain possessed putative enzymes required for glycogen synthesis in bacteria, including 4-alpha-glucan branching enzyme (*GlgB*), and glycogen phosphorylase (*GlgP*), which are responsible for glycogen and starch breakdown.

Four bacteriocins encoding gene clusters as Areas of interest (AOI's) such as streptide, *BlpK*, *BlpU*, and *BlpD* were identified in *S. thermophilus* AARV strain by the BLAST results from the BAGEL4 web server. *BmbF* gene resides beside 295.1 Streptide (start at 72, 0172 and end at 72, 0315) at first AOI. The second AOI includes the bacteriocin genes such as *BlpK*, *BlpU*, and *BlpD*. Two LanT genes encode Bacteriocin ABC exporter and two ABC transporter ATP-binding proteins are located at second AOI. The third AOI includes the *LanB* and *LanC* genes which encode lantibiotic biosynthesis proteins. Lantibiotics are bacteriocins with unique amino acid structures, including lanthionine and  $\beta$ -methyl-lanthionine, generated through post-translational modifications. These changes give lantibiotics their distinct antibacterial capabilities. The fourth AOI includes LanK which encodes the ATPase domains of histidine kinase, DNA gyrase B, and HSP90. LanK is related to the production of lantibiotics. Screening of the entire genome of *S. thermophilus* Sample 2B strain revealed that the first AOI includes bacteriocins encoding gene 295.1 Streptide and the third AOI includes bacteriocin ABC-type exporter (Fig. 3A,B).

The anti-oxidative substances produced by *S. thermophilus*, especially reduced glutathione, may be involved in the advantageous effects of *S. thermophilus* fermented milk products on risk factors for heart disease and hypercholesterolemia, particularly through their ability to protect against low-density lipoprotein oxidation<sup>67</sup>. *S. thermophilus*' genome has evolved to adjust to its environment, specifically milk. Comparative genomics analyses showed considerable gene degradation during sugar consumption and protein delivery, as well as significant lateral gene transfer (LGT) in genes related to exopolysaccharide synthesis, tolerance to stress, and bacteriophage immunity. The species exhibits significant genetic diversity at the strain level, with as many as 5% of genes having known variable functions. This suggests that distinct strains adapt to particular habitats, probably due to selection from human impact. *S. thermophilus* has a distinct lactose absorption system called LacS. This secondary carrier works as both a lactose-galactose antiporter and a lactose/galactose-proton symporter<sup>68</sup>. The Lactose and galactose absorption property of *S. thermophilus* can aid with controlling metabolic diseases caused by lactose and galactose intolerance. *S. thermophilus* strains have genes such as pyruvate-formate lyase (Pfl) that generates formate from pyruvate. This strain also has phosphotransacetylase (*Pta*) and acetate kinase (*AckA*)



**Fig. 3.** Genetic organization of bacteriocin gene clusters in *Streptococcus thermophilus* strains isolated from industrial (A) and home made curd (B) through the BAGEL4 webserver. Red color indicated immunity protein. Streptide: a quorum sensing (QS) regulated macrocyclic peptide, genes such as *BlpK*, *BlpU*, *BlpD* (highlighted in light green colour) involved in bacteriocin production; *LanB* and *LanC* (highlighted in sky blue colour) and *LanK* (highlighted in yellow colour) associated with the biosynthesis and modification of lantibiotics.

that generate acetate. The glutamate decarboxylase enzyme (*GadB*, EC 4.1.1.15) transforms glutamate to GABA, which is released by the *GadC* antiporter. GABA has been linked to health benefits such as antihypertensive, antidiabetic, and diuretic<sup>67</sup>. GABA production by glutamate decarboxylation in bacteria has been linked to acid resistance<sup>55</sup>. The genomes of both *S. thermophilus* strains included complete copies of *lacS* and *lacZ* (Table S7). *S. thermophilus* favors lactose to glucose as its primary carbon and energy resource. Lactose transport and hydrolysis are regulated by the *lac* operon, which is activated in the presence of lactose. The *lac* operon includes lactose permease (*LacS*) and cytoplasmic  $\beta$ -galactosidase (*LacZ*). *LacZ* (EC 3.2.1.23) cleaves lactose into glucose and galactose. Galactose is metabolized to glucose-1-phosphate via the Leloir pathway, which includes the regulator GalR, galactokinase (GalK), galactose-1-phosphate uridylyltransferase (GalT), UDP-glucose-4-epimerase (GalE), and galactosemutarotase. *S. thermophilus* utilizes phosphoenolpyruvate (PEP)-phosphotransferase system (PTS) to absorb carbohydrates. Galactose usage in strains reduces galactose content in dairy products, which benefits human health<sup>69</sup>. Most *S. thermophilus* strains cannot metabolize both free and intracellular galactose, likely due to inadequate activity of the galK and galM genes or alterations in the galR-galK promoter region which affects the level of enzyme expression<sup>32</sup>. The carbohydrate metabolism genes of strains play crucial roles in their ability to use carbohydrates while helping to sugar fermentation<sup>70</sup>. Lactose catabolism produces lactate and other end products, whereas galactose synthesizes polysaccharides, teichoic acids, and nucleotide sugars<sup>67</sup>. *LacZ* may assist in the prevention of colorectal cancer through the prevention of cell proliferation and colony formation, as well as the triggering of cell cycle arrest, and apoptosis in colorectal cancer cells. The anti-tumor actions of *S. thermophilus* are assisted by the capacity of *LacZ* to liberate galactose which disrupts energy balance, stimulating oxidative phosphorylation and inhibiting Hippo pathway kinases<sup>71</sup>. The proteolytic system of *S. thermophilus* includes dipeptidases (*PepV*), aminopeptidase A (*pepA*), aminopeptidase C (*pepC*), and oligoendopeptidase F (*pepF*) etc. (Table S7). As a result, bacteria must use proteins; and generate peptides, and amino acids to meet their nitrogen supply requirements during rapid development in milk<sup>69</sup>. We identified tolerance-related genes in the *S. thermophilus* genome to examine their potential probiotic capabilities. *S. thermophilus* contains bile salt tolerance gene (*bsh*); and genes involved in antioxidant activities such as *dpr*, *nrhH*, *trxA*, *tpx*, *trxB*, *gor*, and *sodA* (Table S7). Probiotic isolates with high antioxidant activity can alleviate oxidative stress. *S. thermophilus* controls iron metabolism to minimize the generation of hazardous reactive oxygen species (ROS)<sup>72</sup>. Methionine sulfoxide reductase B (*msrB*) could be essential to reduce the generation of nitric oxide by cells, which could protect against pathogenic microbes<sup>73</sup>. Arginine (Arg) suppresses the proliferation of the cariogenic bacteria *S. mutans*, influences the outer layer of biofilm by lowering biofilm biomass, generates water-insoluble EPS in the matrix of extracellular cells, and destroys established oral biofilms<sup>74</sup>. The acid-tolerant genes *dapA* and *lysC* modulate lysine production and contribute to the lysine metabolic pathway. The *lysC* gene produces an aspartate kinase, whereas the *dapA* gene encodes a 4-hydroxy-tetrahydrodipicolinate synthase. These two enzymes are necessary for the production of lysine from aspartate and are engaged throughout all the metabolic processes such as those involving succinyl-diaminopimelate (DAP), acetyl-DAP, DAP dehydrogenase, and DAP aminotransferase. Aspartate kinase transforms aspartate to phosphorylated aspartate which has a role in multiple metabolic pathways, including lysine, glycine, serine, threonine, cysteine, and phenylalanine, as well as 2-oxocarboxylate acid metabolism. These genes help strains adapt to their surroundings<sup>75</sup>. The *ureI* gene encodes a pH-dependent urea channel. It is likely induced to compensate for elevated extracellular acidity<sup>25</sup>.

Bacteriocins are ribosome-produced proteins with antibacterial properties that effectively protect against infections and spoilage bacteria, typically targeting strains closely related to the producer or others within the same biological environment. The bacteriocins of *S. thermophilus* showed antibacterial activity against *Bacillus cereus*, *Clostridium botulinum*, *Enterococcus faecalis*, *Enterococcus faecium*, *Escherichia coli*, *Staphylococcus carnosus*, and *Salmonella typhimurium*<sup>67</sup>. Compared with the MD2 and D3 strains, *S. thermophilus* MD8 showed superior antibacterial activity against *Bacillus cereus*, *Escherichia coli*, *Salmonella typhosa*, and *Staphylococcus aureus*, as well as higher levels of  $\beta$ -galactosidase<sup>76</sup>.

Whole-genome sequencing and genomic characterization of both *S. thermophilus* strains revealed genetic variation and additional genes encoding proteins with interesting biotechnological attributes. The genome analysis revealed that both strains have a probiotic gene composition, encoding proteins and enzymes for carbohydrate, nucleotide, and energy metabolism, as well as vitamin and lipid cofactor metabolism and secondary metabolite biosynthesis. The genome research showed that both strains are non-pathogenic, non-virulent, and have a stable genome. CRISPR-Cas systems of both *S. thermophilus* strains can be utilized to create novel strains with improved functional properties. The CRISPR-Cas system is an adaptive immune system that recognizes and cleaves foreign genetic material such as phages and plasmids. Both strains contain the CRISPR-Cas system (Table S5), which may effectively prevent the horizontal transmission of virulence or antibiotic resistance genes.

### Antibiofilm activity of CFS from both *S. thermophilus* strains

Probiotic strains can combat pathogenic bacteria through antimicrobial properties or release chemicals during metabolism<sup>36</sup>. Biofilm creation involves numerous stages, including initial adhesion to a solid surface, reversible attachment, generation of EPS, irreversible attachment, and development into an intricate three-dimensional structure in nature<sup>77</sup>. CFS derived from probiotic strains is being utilized to potentially combat the resistance seen in biofilm-associated infections through the production of antagonistic substances like organic acids, hydrogen peroxide, and bacteriocins, which contribute to antibiofilm action<sup>22</sup>. *Pseudomonas aeruginosa* is recognized as the most alarming pathogen responsible for urinary bladder infections, kidney infections, as well as cystic fibrosis and is estimated to account for 10–20% of all hospital infections, particularly due to its ability to form alarming biofilms<sup>78</sup>. During biofilm growth, *P. aeruginosa* stimulates the release of many virulence agents, including rhamnolipid, pyocyanin, and proteolytic enzymes. Microbial biofilms permit bacteria to propagate disease, either by activating the virulence profile or providing resistance to a wide variety of drugs<sup>19</sup>. *S. aureus* is a widely recognized biofilm-forming Gram-positive bacterium that, in some cases, may act as an opportunistic

microbe<sup>79</sup>. *S. aureus* is responsible for infections such as pneumonia, meningitis, osteomyelitis, abscesses, folliculitis, endocarditis, and cellulitis<sup>80</sup>. These results demonstrated that the CFS of *S. thermophilus* strains from both samples at concentrations ranging from 90 to 60% can effectively reduce the metabolic activity of *S. aureus*, *P. aeruginosa* PAO1, *Acinetobacter baumannii*, and *Klebsiella pneumonia* (Fig. 4A, B). Heating, catalase, and proteinase interventions of CFS did not affect the metabolic activity of bacterial strains. The inhibitory effects of H<sub>2</sub>O<sub>2</sub> and bacteriocins were not noticeable (data not shown). Extracellular polymeric substances (EPS) are a widely utilized biomarker of bacterial biofilm development<sup>81</sup>. The EPS matrix has been found to inhibit the transport of a variety of antibiotics, therefore effectively assisting the bacterial biofilm in remaining alive against various antibiotics<sup>82</sup>. Compared with the control, the nonneutralizing CFS of both *S. thermophilus* strains significantly reduced the EPS production of the investigated bacteria such as *S. aureus*, *P. aeruginosa* PAO1, *A. baumannii*, and *K. pneumonia* (Fig. 4C). Cell-free extracts from probiotic strains may counteract biofilm-related bacterial resistance by producing lactic and acetic acids, which can lower culture pH and potentially serve as an antibacterial mechanism<sup>43</sup>.

When the organisms were cultivated in the presence of various doses of CFS extract, biofilm development decreased substantially compared with that of control. Similarly, when the influence of planktonic cell growth was evaluated, there was substantial reduction in the 600 nm value of the planktonic cell suspension, indicating that the CFS extract also had effect on planktonic cell growth in *S. aureus*, *P. aeruginosa* PAO1, *A. baumannii*, and *K. pneumoniae* (Fig. 4D, E). The inhibitory effects of CFS on *S. aureus*, *P. aeruginosa* PAO1, *A. baumannii*, and *K. pneumoniae* biofilms are shown in (Fig. 4D, E). CFS extracts reduced biofilm development in a dose-dependent fashion. This finding was verified by compound microscopy (Fig. 4F). CFS significantly inhibited biofilm formation by the four strains ( $p < 0.05$ ). The biofilm inhibition rates of CFS-treated *S. aureus* ranged from 90 to 60%, whereas the biofilm inhibition rates of CFS-treated *A. baumannii*, and *K. pneumonia* ranged from 90 to 40%. The inhibition and eradication of biofilms by CFS were examined using the crystal violet (CV) assay (Fig. 4G,H).

#### FT-IR analysis of CFSs of both *S. thermophilus* strains

The FT-IR spectra revealed that various functional groups are present in the CFSs of both strains of *S. thermophilus* (Table S8, Fig.S6). The band at 3176.07 cm<sup>-1</sup> was attributed to a high frequency of hydroxyl groups (O–H groups) and the band at 2927.26 cm<sup>-1</sup> was attributed to a high frequency of methyl (–CH<sub>3</sub>) groups in the CFS of *S. thermophilus* AARV strain. The absorption at 1572.88, 1401.30, and 1116.64 cm<sup>-1</sup> was due to azo compounds (–N=N–), nitrates (NO<sub>3</sub><sup>-</sup>), and ether groups, respectively. The band at 1038.59 cm<sup>-1</sup> confirmed the presence of methylene group (=CH<sub>2</sub>–). The bands at 3193.55 and 2931.30 cm<sup>-1</sup> were assigned to the presence of amide group (–CONH<sub>2</sub>) groups, and methyl groups (–CH<sub>3</sub>) in the CFS of *S. thermophilus* Sample 2B strain respectively. The peak around 1573.41 cm<sup>-1</sup> was attributed to azo compounds (–N=N–). The CFS had absorption peaks at 1401.67 and 1118.05 cm<sup>-1</sup> due to the presence of hydroxyl (–OH) and ether group respectively.

#### GC–MS analysis of CFS from both *S. thermophilus* strains

*S. thermophilus* is a homofermentative bacterium that generates many metabolites, including acetic acid, formic acid, acetaldehyde, and ethanol<sup>83</sup>. The pentose phosphate pathway and TCA cycle of LAB generate a variety of alcohols and acids. In homofermentative LAB, ethanol is generated from pyruvate via acetyl-CoA, but in heterofermentative LAB, it is produced via pentose phosphate route. Compared with heterofermentative LAB, homofermentative LAB had a greater concentration of aldehydes, possibly because of greater alcohol dehydrogenase activity and/or surplus of NADH during development<sup>84</sup>.

The antibiofilm ability of LAB is attributed to metabolites secreted in the surrounding media which are influenced by nutrients in the growth medium<sup>16</sup>. As a result, the chemical composition of the metabolites produced by *S. thermophilus* in the CFS was analyzed by GC–MS, and bioactive components mass spectra were searched in the NIST and Wiley databases. The complete ion chromatogram (TIC) of CFS revealed an abundance of many physiologically active chemicals with varying retention periods. The chemical contents recovered at various time intervals were analyzed using mass spectrometry (MS) to determine their structural diversity. GC–MS analysis revealed 339 chemicals in the CFS of the Sample 2B isolate of *S. thermophilus* and 302 chemicals in the CFS of the AARV isolate of *S. thermophilus*. The major metabolites with the highest component areas included fatty acid esters, branched alkanes, long-chain fatty acids, alpha amino acid esters, phenylpropanes, and secondary alcohols. The antibacterial activity of extracts may be due to the presence of recognized chemical components. The major chemical constituents of the CFS of both isolates were 2, 4-di-tert-butylphenol at retention time (RT) 20.7981, triacontane at RT 32.4752, 1-nonadecene at RT27.1232, succinic acid butyl ethyl ester at RT 18.028, ethyl 2-isocyanato-2-phenylpropionate at RT 27.1655, acetic acid TMS derivative at RT 7.4683, 1-tetradecanol at RT 18.3587, octadecanoic acid at RT 29.1228, and 2-furancarboxamide N-methyl- at RT 5.7737 as evident from the GC–MS spectra. 2-butanol at RT 7.6993, ethyl triacontanate at RT 33.1166, tridecane 7-hexyl- at RT 33.2401, and L-valine, N-ethoxycarbonyl-, methyl ester at RT 7.7335 etc. were detected only in CFS of Sample 2 (Table S9). The functional metabolites significantly enriched the top 25 biological pathways ( $p < 0.05$ ). Metabolite Set Enrichment Analysis identifies biologically significant patterns within quantitative metabolomic data. The hypergeometric test was used in Over Representation Analysis (ORA) to determine if a specific set of metabolites is overrepresented in a compound list. Adjusted for multiple testing, one-tailed *p* values are presented (Fig. S7). Fatty acids and derivatives such as fatty acid methyl ester are renowned for their strong antibacterial and antifungal activities. They are environmentally benign because of their low toxicity, high biodegradability, and resistance to severe temperatures, pH, and salinity. 2, 4-Di-tert-butylphenol has been shown to have strong antioxidant and antitumor properties<sup>85</sup>. All *P. aeruginosa* strains examined require  $\leq 0.31\%$  acetic acid to completely prevent biofilm formation<sup>86</sup>. A derivative of phosphonic acid suppresses bacterial cell wall formation and has a broad spectrum of efficacy against Gram-negative (especially *E. coli* isolates) and

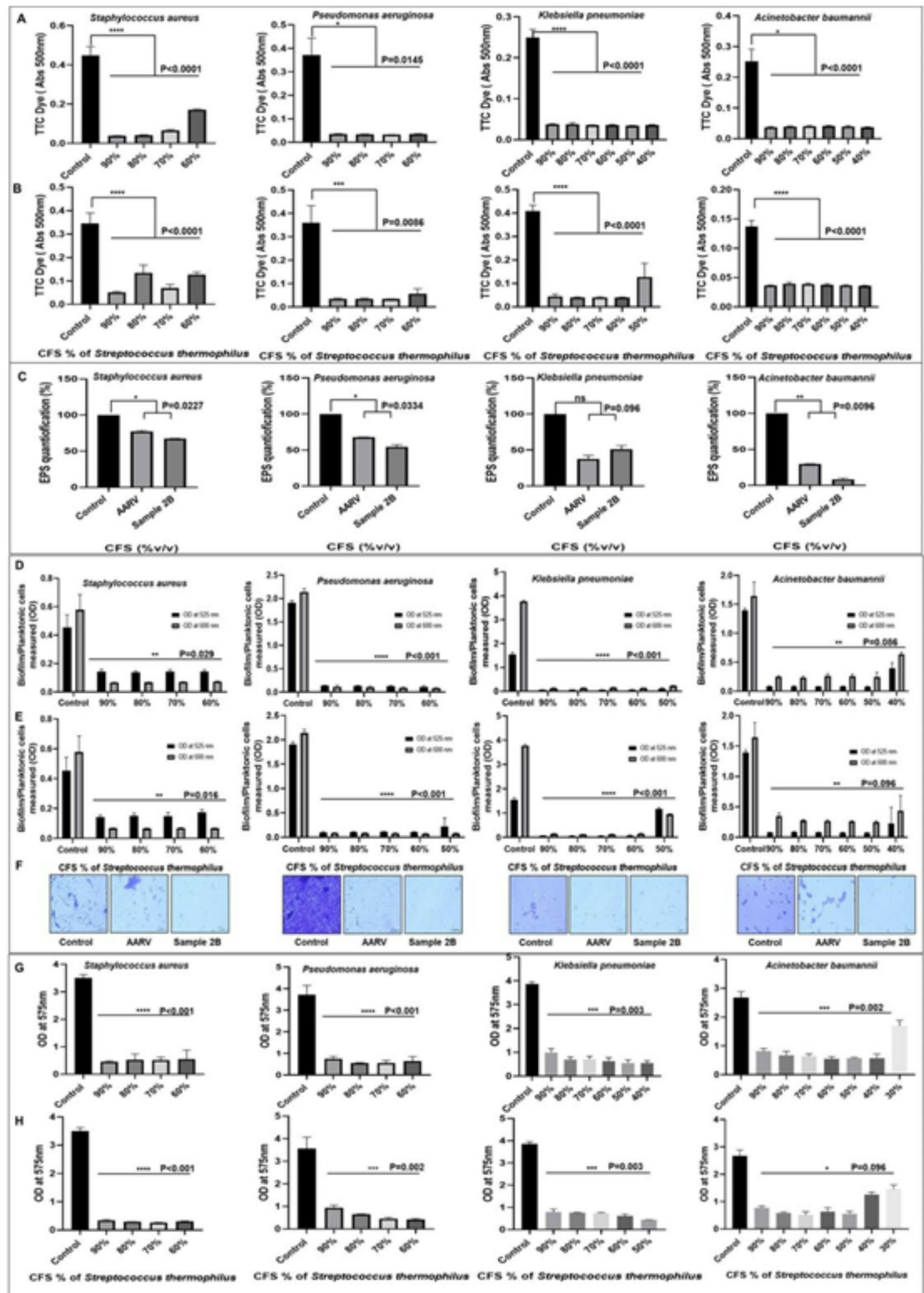


**Fig. 4.** Effect of cell free supernatant (CFS) of *S. thermophilus* strains (A): AARV and (B) Sample 2B on metabolic dye, triphenyl tetrazolium chloride (TTC) metabolism of *S. aureus*, *P. aeruginosa* PAO1, *K. pneumoniae*, and *A. baumannii*. (C) Effect of CFS of *S. thermophilus* strains on EPS production (%) of bacterial biofilm by the phenol-sulphuric acid method. Effects of CFS (%v/v) of *S. thermophilus* strains AARV (D) and Sample 2B (E) on biofilm of *S. aureus*, *P. aeruginosa* PAO1, *K. pneumoniae*, and *A.baumannii* evaluated by crystal violet assay. Planktonic cell growth was measured at 600 nm and biofilm cell growth was measured at 525 nm. (F) Microscopic visualization (×40) of antibiofilm activity of CFS of *S. thermophilus* against the *S. aureus*, *P. aeruginosa*, *K. pneumoniae*, and *A.baumannii* biofilm. Biofilm disrupting potential of CFS of *Streptococcus thermophilus* strains AARV (G) and Sample 2B (H) on preformed biofilms of *S. aureus*, *P. aeruginosa*, *K. pneumoniae*, and *A.baumannii*. Average values of three independent experiments ( $n = 3$ ) and SD are presented. Statistical difference ( $P < 0.05$ ) was measured between control and among CFS treatments.

Gram-positive bacteria, including multidrug-resistant (MDR) strains<sup>87</sup>. Astemizole can prevent ACE2 and block the penetration of SARS-CoV-2 spike pseudovirus into ACE2-expressing HEK293T cells<sup>88</sup>. Succinic acid also demonstrated antibacterial activity against *Proteus mirabilis*<sup>89</sup>.

### ADME, toxicity testing, and Pharmacological activity evaluation

The ADME properties of the metabolites identified in CFS were determined using SWISSADME web server. 2, 4-Di-tert-butylphenol, 2-butanol, succinic acid butyl ethyl ester, 2-furancarboxamide, N-methyl-, phosphonic acid ethyl hexyl ester, 1-norleucine N-methoxycarbonyl-octyl ester, acetic acid TMS derivative, and ethyl 2-isocyanato-2-phenylpropionate satisfied Lipinski's rule of five (Ro5). Molecules have been predicted to exhibit good absorption characteristics. 2-Butanol lacks the blood–brain barrier (BBB) (Table S10). These metabolites may be considered viable therapeutic candidates. To evaluate the toxicity of drug compounds before clinical trials, in-silico techniques should be used. Computational tools for evaluating toxicity are increasingly popular due to their high precision, quickness, and simplicity of application. We evaluated toxicity and side effects using the ProTox-II web server, including the LD50 values, acute, hepatotoxic, cytotoxic, carcinogenic, immunotoxic, and mutagenic characteristics of the metabolites identified in the CFS (Table S11). This examination was carried out to identify the drug-like properties of the chemicals under investigation. The possible biological functions of particular bioactive molecules were investigated utilizing the PASS web server. The PASS analysis results indicate that each of the chemicals has considerable anti-inflammatory activity, antiviral activity, anti-hypoxic activity, oxygen scavenging activity, vasoprotector activity, and platelet aggregation stimulant activity. A Pa value of more than 0.5 indicates an increased possibility of obtaining a target experimental response for a chemical. Specifically, 2, 4-di-tert-butylphenol and 2-butanol presented high Pa values, indicating that their putative pharmaceutical action is larger than other substances (Table S12). 2, 4-di-tert-butylphenol (2, 4-DTBP) may interfere with biofilms by modulating the EPS released from *Serratia marcescens*. This also promotes the distribution of antimicrobials into cell aggregates, leading to the removal of resistant biofilms. It can increase the efficacy of traditional antibiotics. 2, 4-DTBP inhibits quorum sensing (QS)-mediated biofilm development while increasing cell surface hydration, resulting in less biofilm formation. It showed antibacterial activity against two multidrug resistant bacteria *P. aeruginosa* and *S. aureus*. It also inhibited reactive oxygen species (ROS) formation in both *Aspergillus* and *Phytophthora cinnamomi*, indicating a correlation between its antifungal and antioxidative properties. It significantly increased the expression of apoptotic genes (P53 and caspase 7) in cancer cell lines<sup>90</sup>. The drug-likeness measurement obtained from the bioavailable radar plot was assessed using ADMETlab 3.0. Figure S8 displays radar plots illustrating the bioavailabilities of 2-Butanol and 2, 4 Di-tert-butylphenol. The compound 2, 4-Di tertbutyl Phenol exhibited superior size and polarity characteristics compared to 2-Butanol, which resulted in a positive perception of their overall drug-likeness. On the basis of the above in silico analysis, we selected 2, 4-di-tert-butylphenol, and 2-butanol for further molecular docking and dynamics simulation studies against virulent bacterial proteins.

### Molecular Docking and dynamics simulation studies of bacterial virulent proteins with 2, 4-di-tert-butylphenol and 2-butanol

Molecular docking was utilized to investigate the interactions of 2, 4-di-tert-butylphenol and 2-butanol with the target proteins LasI (1RO5), OmpA (3TD4), SasG G51-E-G52 (3TIQ), MrkH (5KED), LasR (6D6P), CsuC-CsuE (6FJY), and AgrC (6E52). LasI promotes the synthesis of plasminogen activator inhibitor-1 (PAI), which aids in the LasI/LasR quorum sensing system in *P. aeruginosa* PAO1<sup>91</sup>. Type 3 fimbriae play a primary role in biofilm formation in *K. pneumoniae*. MrkH in *K. pneumoniae* influences the type 3 fimbriae operon by inducing the MrkA promoter. MrkH is commonly referred to as a “biofilm switch” because it can trigger the transcription of genes involved in the synthesis of type 3 fimbria<sup>92</sup>. AbOmpA influences antimicrobial resistance via the OmpA-like domain in *A. baumannii*<sup>93</sup>. Biofilm generation by *S. aureus* requires cell-surface protein (SasG) that includes sequence repetitions known as G5 domains<sup>94</sup>. The LasR protein is a crucial part of *P. aeruginosa*'s quorum system, providing it with the ability to control biofilm-induced pathogenicity<sup>95</sup>. Biofilm development in *A. baumannii* is facilitated by Csu pili<sup>96</sup>. The accessory gene regulator (agr) quorum-sensing system of *S. aureus* is expected to possess a significant role in biofilm development<sup>97</sup>. To validate the docking results of 2, 4-di-tert-butylphenol and 2-butanol with the target proteins, a molecular dynamics (MD) simulation was performed. The results of the docking studies are shown in (Table 2, Table S13, Fig. 5, and Fig. S9). The best ligands for the target proteins 1RO5, 3TD4, 3TIQ, 5KED, 6D6P, 6FJY, and 6E52 were PubChem CID: 7311 and 6568 respectively. The results of 100 ns molecular dynamics (MD) studies have been shown in (Figs. 6, 7 and 8, and Fig. S10). The configurations of ligands with the highest negative interaction scores were chosen as the optimal binding locations. The relationships between the top-scoring metabolites and target proteins were briefly explained. 2, 4-di-tert-butylphenol had a higher binding affinity than the other chemical tested, resulting in a glide gscore of  $-5.114$  for protein 1RO5,  $-50.46$  for protein 5KED,  $-5.674$  for protein 6D6P,  $-3.231$  for protein 6E52, and  $-4.858$  for protein 6FJY. 2-Butanol had a greater binding affinity than the other chemical tested, resulting in a glide gscore of  $-2.218$  for the protein 3TD4 (Table 2, Table S13).

The molecular docking study of the 1RO5-2, 4-di-tert-butylphenol complex revealed intricate interactions between the ligand and the amino acid residues within the binding site of the target protein (Fig. 5A). The 2, 4-di-tert-butylphenol ligand, featuring aromatic ring structures and tert-butyl functional groups, forms critical interactions mediated by its functional groups. The phenolic hydroxyl group forms a conventional hydrogen bond with the residue ILE107, providing stability to the ligand within the binding pocket. Additionally, Van der Waals interactions are established between the non-polar tert-butyl groups and the hydrophobic residues such as Val148, Asn108, and Ala106, promoting a snug fit of the ligand in the binding site. The presence of Phe117 suggests possible  $\pi$ -alkyl interactions with the aromatic ring of the ligand, further reinforcing its binding orientation. These comprehensive molecular interactions underscore the specificity and stability of the 1RO5-2,

Target protein from bacteria	PDB ID of target protein	Pubchem CID of selected ligands	Ligands name	Glide gscore	Glide emodel (Kcal/mol)	MMGBSA dG bind
AHL synthase lasI (LasI) from <i>Pseudomonas aeruginosa</i> PAO1	1RO5	7311	2,4-Di-tert-butylphenol	-5.114*	-20.246	-36.55
		6568	2-Butanol	-4.060	-16.257	-15.18
OMP-A-like domain from <i>Acinetobacter baumannii</i>	3TD4	7311	2,4-Di-tert-butylphenol	-1.391	-15.262	-20.62
		6568	2-Butanol	-2.218*	-15.133	-18.41
MrkHprotein from <i>Klebsiella pneumonia</i>	5KED	7311	2,4-Di-tert-butylphenol	-50.46*	-28.523	-28.523
		6568	2-Butanol	-3.445	-15.918	-22.65
LasR complex of <i>Pseudomonas aeruginosa</i> PAO1	6D6P	7311	2,4-Di-tert-butylphenol	-5.674*	-30.240	-29.31
		6568	2-Butanol	-2.904	-12.308	-1.07
AgrC protein from <i>Staphylococcus aureus</i>	6E52	7311	2,4-Di-tert-butylphenol	-3.231*	-29.289	-32.3
		6558	2-Butanol	-3.199	-15.668	-21.1
CsuC-CsuE subunit of Csu pili from <i>Acinetobacter baumannii</i>	6FJY	7311	2,4-Di-tert-butylphenol	-4.858*	-0.329	-6.49
		6568	2-Butanol	-3.819	-15.125	-15.74

**Table 2.** Results of virtual screening of selected ligands to the selected target proteins. \*Indicates the highest negative gscore of docking of the metabolites against the target proteins.

4-di-tert-butylphenol complex, driven by a delicate balance of hydrogen bonding, hydrophobic interactions, and ionizable environments within the binding pocket. The 3TD4-2butanol complex reveals intricate interactions between the ligand and specific amino acid residues. The hydroxyl group of the ligand forms conventional hydrogen bonds with THR D: 273 and potential Van der Waals interactions with ARG D: 286 and ASP D: 271 (Fig. 5B). Additionally, the functional groups of the ligand engage in alkyl interactions with LEU D: 278 and LEU D: 282, highlighting the multi-faceted binding dynamics. The presence of hydrogen bond donors and acceptors suggests a robust hydrogen bonding network.

The interaction of the 5KED-2, 4-di-tert-butylphenol complex highlights several critical interactions: Van der Waals forces primarily with Gly144 and Asn34, and Pi-alkyl interactions with Arg65 and His62 (Fig. 5C). The ligand's aromatic ring engages in Pi-alkyl interactions, suggesting stabilization through aromatic stacking with phenylalanine residues, whereas the presence of tert-butyl groups introduces steric bulk, as evidenced by Van der Waals interactions indicative of snug fitting within hydrophobic pockets. The binding surface's attributes such as hydrogen bond donor-acceptor residues, hydrophobicity, and ionizability significantly contribute to the binding affinity. The hydrogen bonding interaction between the ligand and Asn34 (as a conventional hydrogen bond donor) underscores the importance of this binding mode in maintaining complex integrity. These findings illustrate that 5KED-2; 4-di-tert-butylphenol leverages multiple interaction types—hydrophobic, electrostatic, and hydrogen bonding—to achieve a robust binding to its protein target, capitalizing on both the chemical nature of its functional groups and the structural specificity of the amino acids at the binding site.

The 6D6P-2, 4-Di-tert-butylphenol complex reveals intricate interactions between the ligand and the amino acid residues at the binding site of the target protein highlighting the extensive network of Van der Waals, alkyl,  $\pi$ -alkyl, and conventional hydrogen bond interactions (Fig. 5D). The ligand contains various functional groups and ring structures that play a crucial role in binding. Notably, the tert-butyl groups interact primarily through hydrophobic contacts, particularly with leucine residues (D: 39, D: 36, D: 125), emphasizing the hydrophobic nature of this binding site. The aromatic ring systems of the ligand form  $\pi$ -alkyl interactions with residues such as Tyr D: 47 and Val D: 76, adding to the stability of the complex. In addition, the hydroxy group of the ligand engages in hydrogen bonding with The D: 75, suggesting the importance of hydrogen bond donor-acceptor interactions.

A molecular docking study of the 6E52-2, 4-di-tert-butylphenol complex reveals ligand engages with multiple amino acids through various ring structures and functional groups (Fig. 5E). Specifically, the phenolic hydroxyl group forms conventional hydrogen bonds with ASN A: 103, whereas the tert-butyl groups participate in Van der Waals interactions with ALA B: 119 and GLN B: 125. Additionally,  $\pi$ -alkyl interactions are observed with ALA A: 99 and  $\pi$ -cation interactions are observed with ARG B: 55, indicating an extensive network of stabilizing forces.

The 6FJY-2, 4-di-tert-butylphenol complex exhibited a series of interactions predominantly through its aromatic and alkyl ring structures as well as various functional groups (Fig. 5F). The key amino acid residues involved in these interactions include LEU A: 178, LYS A: 179 and ILE A: 207, which form alkyl and Pi-alkyl bonds, enhancing the hydrophobic interactions within the binding pocket. The hydroxyl group of the ligand establishes a conventional hydrogen bond with the ASP A: 208 residue, providing critical stabilization to the ligand-protein complex. The binding surface contains a diverse range of donor and acceptor residues, indicating the potential for strong hydrogen bonding interactions. Overall, the presence of these various interacting residues indicates a robust and multi-faceted interaction complex, making 6FJY-2, 4-di-tert-butylphenol a promising candidate for targeted therapeutics.

The details of the 6FJY-2, 4-di-tert-butylphenol complex are represented in (Fig. 5). Although the docking site is predominately rich in hydrophobic residues, it has H-bond donor and acceptor residues. As a result, the single OH group of 7311 formed a H-bond with ASP A: 208. The ligand is also rich in H-phobic residues (t-butyl group). Therefore, there were alkyl, and pi-alkyl hydrophobic interactions with LEU A: 178, LYS A: 179, LEU A: 189, LEU A: 163, ILE A: 207, and VAL A: 153. Moreover, TRP A: 151 formed one pi-sigma type of interaction.

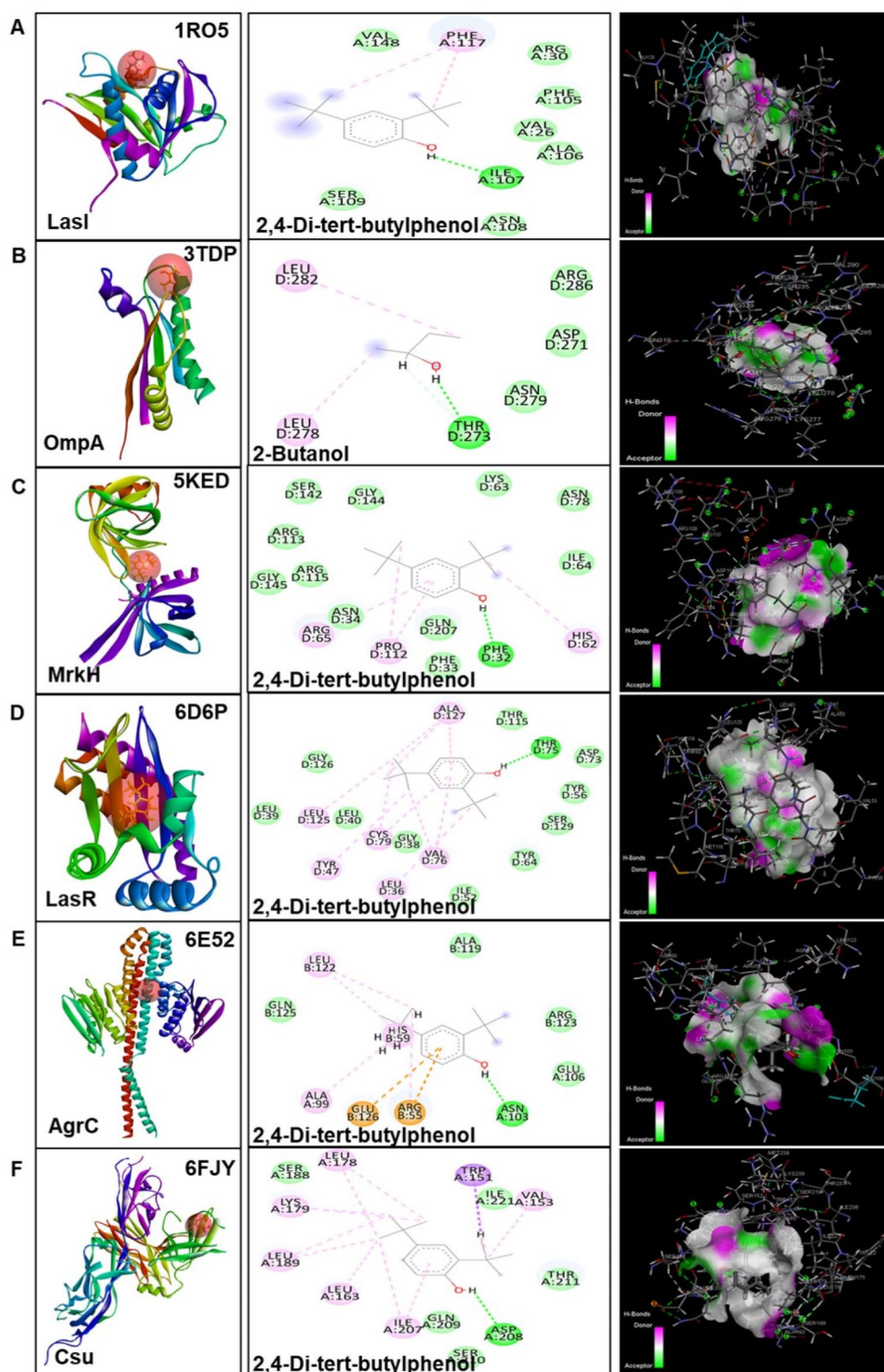


**Fig. 5.** Docking poses and 2D ligand-protein of metabolites (2,4-Di-tert-butylphenol and 2-Butanol) and targeted proteins. **(A)** LasI protein of *P. aeruginosa* PA01, **(B)** OMP-A of *Acinetobacter baumannii*, **(C)** MrkH protein of *Klebsiella pneumoniae*, **(D)** LasR of *P. aeruginosa* PA01, **(E)** AgrC of *S. aureus* and **(F)** Csu of *Acinetobacter baumannii*. The left panel shows the docking poses of ligand binding site of targeted protein, the middle panel shows the 2D interaction diagram of ligand with the protein and right panel displays mapping of binding site cavity according to the presence of H-bond donor-acceptor residue.

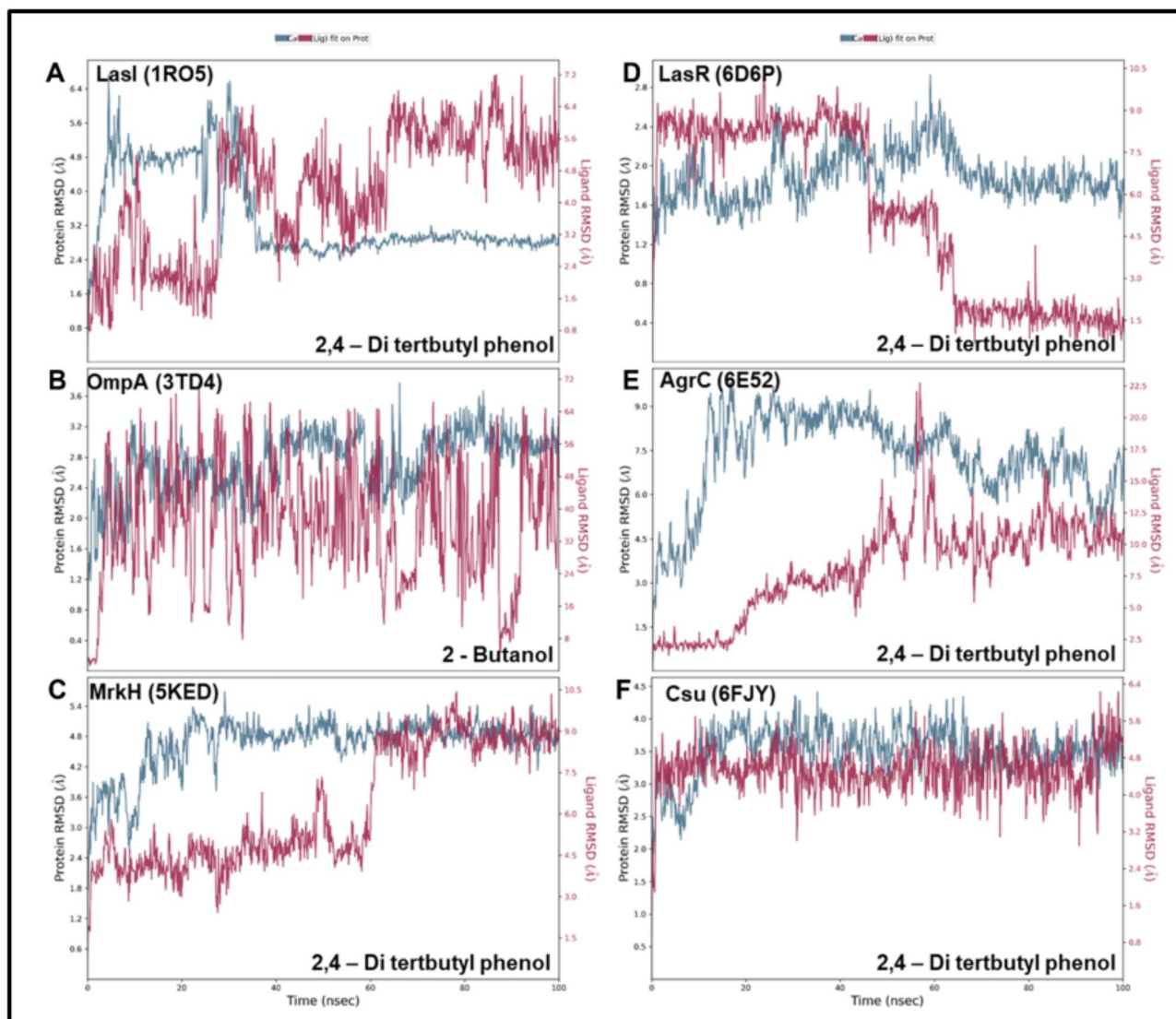


**Fig. 6.** Plot of root mean square deviation (RMSD) of target protein–ligand complexes. (A) LasI protein of *P. aeruginosa* PA01, (B) OMP-A of *Acinetobacter baumannii*, (C) MrkH protein of *Klebsiella pneumoniae*, (D) LasR of *P. aeruginosa* PA01, (E) AgrC of *S. aureus* and (F) Csu of *Acinetobacter baumannii*. The above plot shows the RMSD evolution of a protein (left Y-axis). Ligand RMSD (right Y-axis) indicates how stable the ligand is with respect to the protein and its binding pocket.

As a result, the Glide gscore, Glide emodel, and MMGBSA values were  $-4.858$ ,  $-0.329$  Kcal/mole, and  $-6.49$  Kcal/mole respectively. The Fig S8A–S8F shows the binding site cavity and H-bond donor-acceptor residues, hydrophobic regions, and ionizable areas for each protein–ligand complex.

The protein–ligand complexes of target proteins 1RO5, 5KED, 6D6P, 6E52, and 6FJY with metabolites, 2, 4 – di tertbutyl phenol and 3TD4 with metabolite 2-butanol in their most favourable docking position were simulated for 100 ns using the molecular dynamic simulation (MDS) method. This approach was one of the most widely used *in silico* techniques for analyzing the composition and the binding location within the receptor-binding region<sup>52</sup>. The study examined various variables, including the root mean square deviation (RMSD), root mean square fluctuation (RMSF), number of hydrogen bonds, radius of gyration (Rg), solvent accessible surface area (SASA), polar surface area (PSA), and molecular surface area (MolSA) over a 100 ns molecular dynamic simulation for all complexes. The molecular dynamics simulation revealed a significant level of structural compactness and stability for each of them, as observed over a 100-ns time step. Analysis of the trajectory involved calculating RMSD, RMSF, Rg, and the number of hydrogen bonds after conducting the MD simulation. The root mean square RMSD is a quantitative measure that assesses the degree to which the average configuration of a molecule deviates from a reference configuration, especially the original protein structure at the beginning of the simulation. A greater RMSD indicates that the protein structure is less stable and has undergone more substantial conformational changes during the simulation<sup>98</sup>. The proteins 1RO5, 3TD4, and 6D6P exhibited consistent stability throughout the simulation, as indicated by their RMSD values remaining

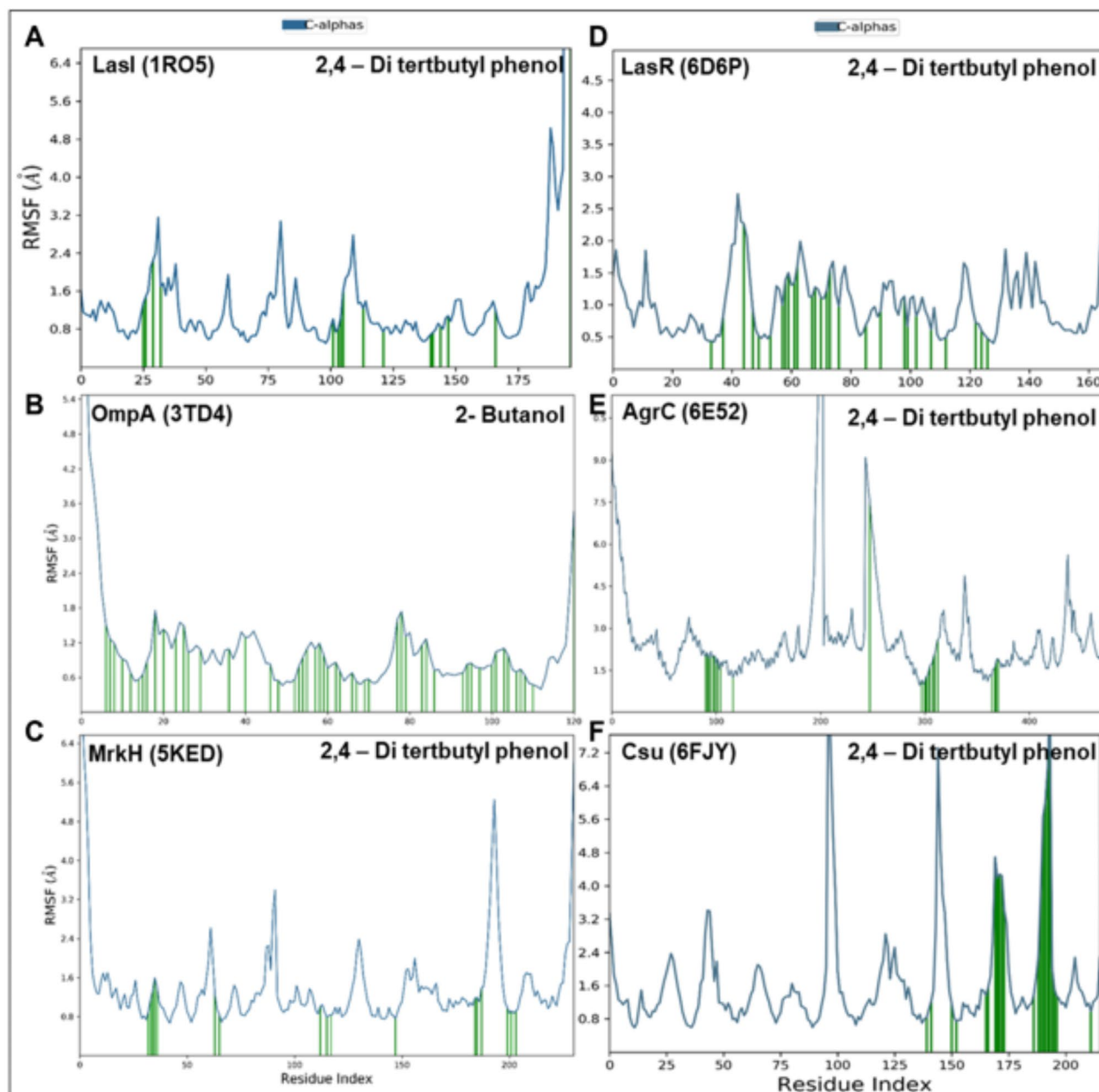


**Fig. 7.** Plot of root mean square fluctuations (RMSF) of target protein–ligand complexes. **(A)** LasI protein of *P. aeruginosa* PA01, **(B)** OMP-A of *Acinetobacter baumannii*, **(C)** MrkH protein of *Klebsiella pneumoniae*, **(D)** LasR of *P. aeruginosa* PA01, **(E)** AgrC of *S. aureus* and **(F)** Csu of *Acinetobacter baumannii*. Protein residues that interact with the ligand are marked with green-coloured vertical bars.

within a range of 2–3 Å (Fig. 6A, B,D). It can be deduced that structure of the proteins slightly changed during the simulation. However, the protein 3TD4\_2-butanol complex presented a relatively higher ligand RMSD of 36.58 Å on average, which is an unacceptable range of RMSD values. The values found are significantly greater than the protein's RMSD, indicating that the ligand moved away from its original binding site. A higher RMSD indicates that the ligand structure is fluctuating more suggesting weaker ligand interaction with the protein (Fig. 6B). Proteins 5KED and 6E52 substantially increased in RMSD throughout the simulation, eventually reaching values of around 4–5 Å (Fig. 6C, E). These data suggest that the proteins have undergone substantial changes in their shape, which may lead to decreased stability. The protein 6FJY demonstrated a substantial increase in the RMSD, of approximately 7 Å at the end of the simulation and exhibited ligand RMSD average value of 3.93 Å which is the lowest value compared to other proteins (Fig. 6F). These findings suggest that the protein has undergone significant changes in form and has the least amount of stability compared to the other six proteins that were tested.



The radius of gyration ( $R_g$ ) is an essential parameter used to assess the rigidity and flexibility of MDS systems. The hardness of the protein structure was estimated using the  $R_g$ . The target protein-ligand complex was tested to determine the impact of the metabolites on the overall protein flexibility. It has been found that for the target proteins (1RO5, 5KED, 6D6P, 6E52, 6FJY) with the ligand 2, 4-di-tertbutyl phenol exhibited a range of 2.80 to 2.90 Å throughout the simulation (Fig S9A). For the target protein 3TD4 with ligand 2-Butanol the  $R_g$  ranges only from 1.50 to 1.72 Å indicating the least interaction with the protein. A low solvent-accessible surface area (SASA) of 10.679–170.902 Å<sup>2</sup>, a low PSA (polar surface area) of 30.24–35.86 Å<sup>2</sup> and highMolSA (molecular surface area) of 230.159–240.451 Å<sup>2</sup>, were also found in the 2,4 – di-tertbutyl phenol molecule with target proteins, which helped to ensure its stability throughout a 100 ns MD simulation. In contrast, the ligand 2-butanol has a exhibits a high solvent-accessible surface area (SASA) with an average of 228.902 Å<sup>2</sup>, a high PSA (polar surface area) with an average of 42.14 Å<sup>2</sup> and lowMolSA (molecular surface area) with an average of 109.159–Å<sup>2</sup> respectively, indicating the lower stability of the molecule (Fig S9B–D)<sup>100</sup>.

The results of MD simulations of the complexes revealed water-bridge, hydrogen bonding, ionic bonding, and hydrophobic interactions within the stable binding pocket regions. For protein 1RO5, the residues VAL26, ARG 30, PHE105, and ILE107 exhibited hydrogen bonding with water bridges and hydrophobic interactions. ILE107 has hydrophobic as well as water-bridge interactions, plays a substantial role in the active binding site and is crucial for the stability of the ligand 2, 4-di tertbutyl phenol (Fig. 8A). However, for the protein 3TD4, many interacting residues formed hydrogen bonds with water bridges, indicating that the ligand 2-butanol does not facilitate the specific interactions at the active binding site of the protein, indicating a relatively low stability of the protein-ligand complex (Fig. 8B). For the protein 5KED, the residues ASN35, ARG115, LYS184, and ASN185 displayed ionic bond interaction along with water bridges (Fig. 8C), and 6FJY presented fewer ionic bond interactive residues, namely, LYS179, LYS191, SER210, and THR211 with the ligand 2, 4 – di tertbutyl phenol of the active binding site (Fig. 8F). The target proteins 6D6P and 6E52 displayed several hydrogen bonds with good frequencies throughout the simulation (Fig. 8D, E). The hydrogen bonding was evaluated throughout the simulation, and the results indicated that ligand 2; 4-di tertbutyl phenol has an inhibitory effect due to the presence of additional water bridges.

## Conclusions

This study examined the efficacy, genomic characteristics, and probiotic capabilities of two *S. thermophilus* strains obtained from homemade and industrial curd. Whole-genome sequencing and in vitro assays were used to assess the critical elements of probiotic efficacy, including environmental tolerance, antibacterial activity, and biofilm-disrupting characteristics. Both *S. thermophilus* strains showed remarkable resistance to adverse environmental conditions such as acidic pH, bile salts, high salt concentrations, and phenolic chemicals. They also showed no haemolytic or DNase activity, suggesting the absence of pathogenic capability. The strains showed excellent adherence abilities (autoaggregation, coaggregation, and hydrophobicity), which are essential for their probiotic capabilities in the gut. Furthermore, these compounds exhibit substantial antioxidant activity, which can help with gut health and prevent oxidative stress. A genome study revealed genes associated with important probiotic activities such as survival under acidic and bile stress, adaptability to temperature fluctuations, the oxidative stress response, and bacteriocin production. The study revealed that CFS from both *S. thermophilus* strains could efficiently break biofilms generated by pathogenic bacteria such as *S. aureus*, *K. pneumoniae*, *A. baumannii*, and *P. aeruginosa*. GC-MS analysis revealed bioactive compounds in the CFS, including 2, 4-di-tert-butylphenol and 2-butanol, which have strong pharmacological activity, especially in the inhibition of biofilm development. In silico study confirmed the link between these metabolites and bacterial virulence genes associated with biofilm development. In conclusion, this study demonstrates the diverse probiotic capabilities of *S. thermophilus* strains isolated from curd, particularly their biofilm-disrupting and antibacterial properties, and provides novel insights into their genomic and metabolic characteristics which support their implementation in effective probiotic use.

## Data availability

All data supporting the findings of the study are available within the main manuscript text and supplementary file ( Supplementary file by Dr. Indranil.doc). Sequence data that support the findings of this study have been deposited in the NCBI-SRA database with the accession number PRJNA1190944.

Received: 23 July 2024; Accepted: 17 February 2025

Published online: 27 February 2025

## References

- Goel, A., Halami, P. M. & Tamang, J. P. Genome analysis of *Lactobacillus plantarum* isolated from some Indian fermented foods for bacteriocin production and probiotic marker genes. *Front. Microbiol.* **11**, 40 <https://doi.org/10.3389/fmicb.2020.00040> (2020).
- Taj, R. et al. In vitro screening of EPS-producing *Streptococcus thermophilus* strains for their probiotic potential from Dahi. *Food Sci. Nutr.* **10** (7), 2347–2359. <https://doi.org/10.1002/fsn3.2843> (2022).
- Tamang, J. P., Shin, D. H., Jung, S. J. & Chae, S. W. Functional properties of microorganisms in fermented foods. *Front. Microbiol.* **7**, 578. <https://doi.org/10.3389/fmicb.2016.00578> (2016).
- Liu, W. et al. Characterization of potentially probiotic lactic acid bacteria and bifidobacteria isolated from human colostrum. *J. Dairy. Sci.* **103** (5), 4013–4025. <https://doi.org/10.3168/jds.2019-17602> (2020).
- Yadav, M. & Mandeep, Shukla, P. Probiotics of diverse origin and their therapeutic applications: A review. *J. Am. Coll. Nutr.* **39** (5), 469–479. <https://doi.org/10.1080/07315724.2019.1691957> (2020).
- Yadav, M. & Sunita, Shukla, P. Probiotic potential of *Weissella paramesenteroides* MYPS5.1 isolated from customary dairy products and its therapeutic application. *3 Biotech.* **12** (1), 9. <https://doi.org/10.1007/s13205-021-03074-2> (2022).
- Soliamani, O., Salimi, F. & Rezaei, A. Characterization of exopolysaccharide produced by probiotic enterococcus durans DU1 and evaluation of its anti-biofilm activity. *Arch. Microbiol.* **204** (7), 419 (2022).

8. Somashekaraiah, R., Shruthi, B., Deepthi, B. V. & Sreenivasa, M. Y. Probiotic properties of lactic acid bacteria isolated from Neera: A naturally fermenting coconut palm nectar. *Front. Microbiol.* **10**, 1382. <https://doi.org/10.3389/fmicb.2019.01382> (2019).
9. Ramos, C. L., Thorsen, L., Schwan, R. F. & Jespersen, L. Strain-specific probiotics properties of *Lactobacillus fermentum*, *Lactobacillus plantarum* and *Lactobacillus brevis* isolates from Brazilian food products. *Food Microbiol.* **36** (1), 22–9. <https://doi.org/10.1016/j.fm.2013.03.010> (2013).
10. Kumari, V. B. C. et al. Evaluation of probiotic and antidiabetic attributes of *Lactobacillus* strains isolated from fermented beetroot. *Front. Microbiol.* **13**, 911243. <https://doi.org/10.3389/fmicb.2022.911243> (2022).
11. Aziz, T. et al. Integrated genome based evaluation of safety and probiotic characteristics of *Lactiplantibacillus plantarum* YW11 isolated from Tibetan Kefir. *Front. Microbiol.* **14**, 1157615. <https://doi.org/10.3389/fmicb.2023.1157615> (2023).
12. Aziz, T. et al. Genome investigation and functional annotation of *Lactiplantibacillus plantarum* YW11 revealing streptin and ruminococcin-A as potent nutritive bacteriocins against gut symbiotic pathogens. *Molecules* **28** (2), 491. <https://doi.org/10.3390/molecules28020491> (2023).
13. Aziz, T. et al. Assessing the probiotic potential, antioxidant, and antibacterial activities of oat and soy milk fermented with *Lactiplantibacillus plantarum* strains isolated from Tibetan Kefir. *Front. Microbiol.* **14**, 1265188. <https://doi.org/10.3389/fmicb.2023.1265188> (2023).
14. Aziz, T. et al. Functional annotation of *Lactiplantibacillus plantarum* 13–3 as a potential starter probiotic involved in the food safety of fermented products. *Molecules* **27** (17), 5399. <https://doi.org/10.3390/molecules27175399> (2022).
15. Aziz, T. et al. Assessment of the whole genome sequencing of *Lactiplantibacillus plantarum* 13–3 for Elucidation of novel bacteriocin producing gene cluster and confirmation of its potential probiotic functionality and safety applications. *CyTA - J. Food.* **22** (1). <https://doi.org/10.1080/19476337.2024.2329753> (2024).
16. Nataraj, B. H., Ali, S. A., Behare, P. V. & Yadav, H. Postbiotics-parabiotics: the new horizons in microbial biotherapy and functional foods. *Microb. Cell. Fact.* **19** (1), 168. <https://doi.org/10.1186/s12934-020-01426-w> (2020).
17. Peng, M. et al. Effectiveness of probiotics, prebiotics, and prebiotic-like components in common functional foods. *Compr. Rev. Food Sci. Food Saf.* **19** (4), 1908–1933. <https://doi.org/10.1111/1541-4337.12565> (2020).
18. Yadav, R., Puniya, A. K. & Shukla, P. Probiotic properties of *Lactobacillus plantarum* RYPR1 from an Indigenous fermented beverage Raabadi. *Front. Microbiol.* **7**, 1683. <https://doi.org/10.3389/fmicb.2016.01683> (2016).
19. Gupta, P., Sarkar, S., Das, B., Bhattacharjee, S. & Tribedi, P. Biofilm, pathogenesis and prevention—A journey to break the wall: a review. *Arch. Microbiol.* **198** (1), 1–15. <https://doi.org/10.1007/s00203-015-1148-6> (2016).
20. Chakraborty, P. et al. 3,6-Di(pyridin-2-yl)-1,2,4,5-tetrazine (pytz)-capped silver nanoparticles (TzAgNPs) inhibit biofilm formation of *Pseudomonas aeruginosa*: a potential approach toward breaking the wall of biofilm through reactive oxygen species (ROS) generation. *Folia Microbiol. (Praha)* **63** (6), 763–772. <https://doi.org/10.1007/s12223-018-0620-5> (2018).
21. Paul, P. et al. 1, 4-naphthoquinone efficiently facilitates the disintegration of pre-existing biofilm of *Staphylococcus aureus* through eDNA intercalation. *Folia Microbiol. (Praha)* **68** (6), 843–854. <https://doi.org/10.1007/s12223-023-01053-z> (2023).
22. Fernandes, M. S. M. et al. Effect of *Lactobacillus* spp. cell-free supernatant against planktonic growth and biofilm formation of foodborne *Escherichia coli* isolates. *Lett. Appl. Microbiol.* **76** (1), ovac006. <https://doi.org/10.1093/lambio/ovac006> (2023).
23. Apiwatsiri, P. et al. Anticonjugation and antibiofilm evaluation of probiotic strains *Lactobacillus plantarum* 22F, 25F, and *Pediococcus acidilactici* 72 N against *Escherichia coli* harboring *mcr-1* gene. *Front. Vet. Sci.* **8**, 614439. <https://doi.org/10.3389/fvets.2021.614439> (2021).
24. Zarin Taj, A., Sudheer, V., Vivekananthan & Indranil Chattopadhyay. In Silico and in vitro approach to assessing the antimicrobial efficiency of novel AMP variants derived from *Lactobacillus* Sp. against ESKAPE pathogens. *Biocatal. Agric. Biotechnol.* **58**, 103235. <https://doi.org/10.1016/j.bcab.2024.103235> (2024).
25. Alexandraki, V. et al. Comparative genomics of *Streptococcus thermophilus* support important traits concerning the evolution, biology and technological properties of the species. *Front. Microbiol.* **10**, 2916. <https://doi.org/10.3389/fmicb.2019.02916> (2019).
26. Liu, Q. et al. Genomic and phenotypic-based safety assessment and probiotic properties of *Streptococcus thermophilus* FUA329, a urolithin A-producing bacterium of human milk origin. *Genomics* **115** (6), 110724. <https://doi.org/10.1016/j.ygeno.2023.110724> (2023).
27. Tenea, G. N. & Hurtado, P. Next-generation sequencing for whole-genome characterization of *Weissella cibaria* UTNG210 strain originated from wild *Solanum tomentosum* lam. Fruits: an atlas of metabolites with biotechnological significance. *Front. Microbiol.* **12**, 675002. <https://doi.org/10.3389/fmicb.2021.675002> (2021).
28. Monika, S., Kumar, V., Kumari, A., Angmo, K. & Bhalla, T. C. Isolation and characterization of lactic acid bacteria from traditional pickles of Himachal Pradesh, India. *J. Food Sci. Technol.* **54** (7), 1945–1952. <https://doi.org/10.1007/s13197-017-2629-1> (2017).
29. Tamura, K., Stecher, G. & Kumar, S. MEGA11: molecular evolutionary genetics analysis version 11. *Mol. Biol. Evol.* **38** (7), 3022–3027. <https://doi.org/10.1093/molbev/msab120> (2021).
30. Rai, R. & Tamang, J. P. In vitro and genetic screening of probiotic properties of lactic acid bacteria isolated from naturally fermented cow-milk and yak-milk products of Sikkim, India. *World J. Microbiol. Biotechnol.* **38** (2), 25. <https://doi.org/10.1007/s11274-021-03215-y> (2022).
31. Gharbi, Y. et al. In-vitro characterization of potentially probiotic *Lactobacillus* strains isolated from human microbiota: interaction with pathogenic bacteria and the enteric cell line HT29. *Ann. Microbiol.* **69**, 61–72. <https://doi.org/10.1007/s13213-018-1396-1> (2019).
32. Ragul, K., Syiem, I., Sundar, K. & Shetty, P. H. Characterization of probiotic potential of *Bacillus* species isolated from a traditional Brine pickle. *J. Food Sci. Technol.* **54** (13), 4473–4483. <https://doi.org/10.1007/s13197-017-2928-6> (2017).
33. Jaiswal, S., Pradhan, S. N., Jain, D., Dhassiah Peter, M. P. & Antony, U. Probiotic and functional characterization of *Pediococcus acidilactici* isolated from bhaati Jaanr, traditional fermented rice porridge. *Appl. Biochem. Biotechnol.* **194** (12), 5734–5747. <https://doi.org/10.1007/s12010-022-04041-0> (2022).
34. Pan, W. H., Li, P. L. & Liu, Z. The correlation between surface hydrophobicity and adherence of *Bifidobacterium* strains from centenarians' faeces. *Anaerobe* **12** (3), 148–152. <https://doi.org/10.1016/j.anaerobe.2006.03.001> (2006).
35. Shangliang, H. N., Sharma, S., Rai, R. & Tamang, J. P. Some technological properties of lactic acid bacteria isolated from Dahi and Datshi, naturally fermented milk products of Bhutan. *Front. Microbiol.* **8**, 116. <https://doi.org/10.3389/fmicb.2017.00116> (2017).
36. Rocha-Ramírez, L. M., Hernández-Chiñas, U., Moreno-Guerrero, S. S., Ramírez-Pacheco, A. & Eslava, C. A. Probiotic properties and Immunomodulatory activity of *Lactobacillus* strains isolated from dairy products. *Microorganisms* **9** (4), 825. <https://doi.org/10.3390/microorganisms9040825> (2021).
37. Sophatha, B., Piwat, S. & Teanpaisan, R. Adhesion, anti-adhesion and aggregation properties relating to surface charges of selected *Lactobacillus* strains: study in Caco-2 and H357 cells. *Arch. Microbiol.* **202** (6), 1349–1357 (2020).
38. Zawistowska-Rojek, A., Kośmider, A., Stepień, K. & Tyski, S. Adhesion and aggregation properties of *Lactobacillaceae* strains as protection ways against enteropathogenic bacteria. *Arch. Microbiol.* **204** (5), 285. <https://doi.org/10.1007/s00203-022-02889-8> (2022).
39. Morais, D. A. A., Cavalcante, J. V. F., Monteiro, S. S., Pasquali, M. A. B. & Dalmolin, R. J. S. MEDUSA: A pipeline for sensitive taxonomic classification and flexible taxonomic annotation of metagenomic shotgun sequences. *Front. Genet.* **13**, 814437. <https://doi.org/10.3389/fgene.2022.814437> (2022).
40. Seemann, T. Prokka: rapid prokaryotic genome annotation. *Bioinformatics* **30** (14), 2068–2069. <https://doi.org/10.1093/bioinformatics/btu153> (2014).

41. Cantalapiedra, C. P., Hernández-Plaza, A., Letunic, I., Bork, P. & Huerta-Cepas, J. eggNOG-mapper v2: functional annotation, orthology assignments, and domain prediction at the metagenomic scale. *Mol. Biol. Evol.* **8** (12), 5825–5829. <https://doi.org/10.1093/molbev/msab293> (2021).
42. Stergiou, O. S. et al. Whole-genome sequencing, phylogenetic and genomic analysis of *Lactiplantibacillus pentosus* L33, a potential probiotic strain isolated from fermented sausages. *Front. Microbiol.* **12**, 746659. <https://doi.org/10.3389/fmicb.2021.746659> (2021).
43. Chen, C. C. et al. Antimicrobial ability and mechanism analysis of *Lactobacillus* species against carbapenemase-producing enterobacteriaceae. *J. Microbiol. Immunol. Infect.* **54** (3), 447–456. <https://doi.org/10.1016/j.jmii.2020.01.005> (2021).
44. Haney, E. F., Trimble, M. J., Cheng, J. T., Vallé, Q. & Hancock, R. E. W. Critical assessment of methods to quantify biofilm growth and evaluate antibiofilm activity of host defence peptides. *Biomolecules* **8** (2), 29. <https://doi.org/10.3390/biom8020029> (2018).
45. Das, S. et al. Piperine, a plant alkaloid, exhibits efficient disintegration of the pre-existing biofilm of *Staphylococcus aureus*: a step towards effective management of biofilm threats. *Appl. Biochem. Biotechnol.* <https://doi.org/10.1007/s12010-023-04610-x> (2023).
46. Rossoni, R. D. et al. Inhibitory effect of probiotic *Lactobacillus* supernatants from the oral cavity on *Streptococcus mutans* biofilms. *Microb. Pathog.* **123**, 361–367. <https://doi.org/10.1016/j.micpath.2018.07.032> (2018).
47. Martiz, R. M. et al. Inhibition of carbohydrate hydrolyzing enzymes by a potential probiotic *Levilactobacillus brevis* RAMULAB49 isolated from fermented *Ananas comosus*. *Front. Microbiol.* **14**, 1190105. <https://doi.org/10.3389/fmicb.2023.1190105> (2023).
48. Kumari, V. B. C. et al. Antidiabetic activity of potential probiotics *Limosilactobacillus* spp., *Levilactobacillus* spp., and *Lactocaseibacillus* spp. Isolated from fermented sugarcane juice: A comprehensive in vitro and in silico study. *Nutrients* **15** (8), 1882. <https://doi.org/10.3390/nu15081882> (2023).
49. Harder, E. et al. OPLS3: A force field providing broad coverage of drug-like small molecules and proteins. *J. Chem. Theory Comput.* **12** (1), 281–296. <https://doi.org/10.1021/acs.jctc.5b00864> (2016).
50. Waszkowycz, B. Towards improving compound selection in structure-based virtual screening. *Drug Discov Today* **13** (5–6). <https://doi.org/10.1016/j.drudis.2007.12.002> (2008), 219–26.
51. Ghosh, D. et al. Computational prediction of the molecular mechanism of Statin group of drugs against SARS-CoV-2 pathogenesis. *Sci. Rep.* **12** (1), 6241. <https://doi.org/10.1038/s41598-022-09845-y> (2022).
52. Taj, Z. & Chattopadhyay, I. Identification of bio-active secondary metabolites from Actinobacteria as potential drug targets against *Porphyromonas gingivalis* in oral squamous cell carcinoma using molecular Docking and dynamics study. *Silico Pharmacol.* **12**, 34. <https://doi.org/10.1007/s40203-024-00209-0> (2024).
53. Shivangi, S., Devi, P. B., Ragul, K. & Shetty, P. H. Probiotic potential of bacillus strains isolated from an acidic fermented food Idli. *Probiotics Antimicrob. Proteins* **12** (4), 1502–1513. <https://doi.org/10.1007/s12602-020-09650-x> (2020).
54. Soares, M. B. et al. The resistance of bacillus, bifidobacterium, and Lactobacillus strains with claimed probiotic properties in different food matrices exposed to simulated Gastrointestinal tract conditions. *Food Res. Int.* **125**, 108542. <https://doi.org/10.1016/j.foodres.2019.108542> (2019).
55. Naissinger da Silva, M., Tagliapietra, B. L., Flores, V. D. A. & Pereira Dos Santos Richards NS. In vitro test to evaluate survival in the Gastrointestinal tract of commercial probiotics. *Curr. Res. Food Sci.* **4**, 320–325. <https://doi.org/10.1016/j.crfs.2021.04.006> (2021).
56. Singh, S. et al. Probiotic attributes and prevention of LPS-induced pro-inflammatory stress in RAW264.7 macrophages and human intestinal epithelial cell line (Caco-2) by newly isolated *Weissella cibaria* strains. *Food Funct.* **9** (2), 1254–1264. <https://doi.org/10.1039/c7fo00469a> (2018).
57. Yasmin, I. et al. In vitro probiotic potential and safety evaluation (hemolytic, cytotoxic activity) of *Bifidobacterium* strains isolated from Raw camel milk. *Microorganisms* **8** (3), 354. <https://doi.org/10.3390/microorganisms8030354> (2020).
58. Zhang, J. et al. First insight into the probiotic properties of ten *Streptococcus thermophilus* strains based on in vitro conditions. *Curr. Microbiol.* **77** (3), 343–352. <https://doi.org/10.1007/s00284-019-01840-3> (2020).
59. Patel, A., Prajapati, J., Holst, O. & Ljungh, A. Determining probiotic potential of exopolysaccharide producing lactic acid bacteria isolated from vegetables and traditional Indian fermented food products. *Food Biosci.* **5**, 27–33 (2014).
60. Li, M. et al. Characterization of lactic acid bacteria isolated from the Gastrointestinal tract of a wild Boar as potential probiotics. *Front. Vet. Sci.* **7**, 49. <https://doi.org/10.3389/fvets.2020.00049> (2020).
61. Dey, D. K., Khan, I. & Kang, S. C. Anti-bacterial susceptibility profiling of *Weissella confusa* DD\_A7 against the multidrug-resistant ESBL-positive *E. coli*. *Microb. Pathog.* **128**, 119–130. <https://doi.org/10.1016/j.micpath.2018.12.048> (2019).
62. Montoro, B. P. et al. Fermented Aloréña table olives as a source of potential probiotic *Lactobacillus pentosus* strains. *Front. Microbiol.* **7**, 1583. <https://doi.org/10.3389/fmicb.2016.01583> (2016).
63. Zheng, M. et al. Assessing the risk of probiotic dietary supplements in the context of antibiotic resistance. *Front. Microbiol.* **8**, 908. <https://doi.org/10.3389/fmicb.2017.00908> (2017).
64. Li, A. et al. Probiotics isolated from Yaks improves the growth performance, antioxidant activity, and cytokines related to immunity and inflammation in mice. *Microb. Cell. Fact.* **18** (1), 112. <https://doi.org/10.1186/s12934-019-1161-6> (2019).
65. Hu, T., Cui, Y., Zhang, Y., Qu, X. & Zhao, C. Genome analysis and physiological characterization of four *Streptococcus thermophilus* strains isolated from Chinese traditional fermented milk. *Front. Microbiol.* **11**, 184. <https://doi.org/10.3389/fmicb.2020.00184> (2020).
66. Liu, B. et al. Probiotic potential and safety assessment of *Lactiplantibacillus plantarum* cqf-43 and whole-genome sequence analysis. *Int. J. Mol. Sci.* **24** (24), 17570. <https://doi.org/10.3390/ijms242417570> (2023).
67. Roux, E. et al. The genomic basis of the *Streptococcus thermophilus* health-promoting properties. *BMC Genom.* **23** (1), 210. <https://doi.org/10.1186/s12864-022-08459-y> (2022).
68. Markakiou, S., Gaspar, P., Johansen, E., Zeidan, A. A. & Neves, A. R. Harnessing the metabolic potential of *Streptococcus thermophilus* for new biotechnological applications. *Curr. Opin. Biotechnol.* **61**, 142–152. <https://doi.org/10.1016/j.copbio.2019.12.019> (2020).
69. Cui, Y. et al. New insights into various production characteristics of *Streptococcus thermophilus* strains. *Int. J. Mol. Sci.* **17** (10), 1701. <https://doi.org/10.3390/ijms17101701> (2016).
70. Cui, Y., Wang, M., Zheng, Y., Miao, K. & Qu, X. The carbohydrate metabolism of *Lactiplantibacillus plantarum*. *Int. J. Mol. Sci.* **22** (24), 13452. <https://doi.org/10.3390/ijms222413452> (2021).
71. Li, Q. et al. *Streptococcus thermophilus* inhibits colorectal tumorigenesis through secreting  $\beta$ -galactosidase. *Gastroenterology* **160** (4), 1179–1193e14. <https://doi.org/10.1053/j.gastro.2020.09.003> (2021).
72. Sieuwerts, S. et al. Mixed-culture transcriptome analysis reveals the molecular basis of mixed-culture growth in *Streptococcus thermophilus* and *Lactobacillus bulgaricus*. *Appl. Environ. Microbiol.* **76** (23), 7775–7784. <https://doi.org/10.1128/AEM.01122-10> (2010).
73. Smythe, P. & Efthimiou, G. In Silico genomic and metabolic atlas of *Limosilactobacillus reuteri* DSM 20016: an insight into human health. *Microorganisms* **10** (7), 1341. <https://doi.org/10.3390/microorganisms10071341> (2022).
74. Bijle, M. N., Ekambaram, M., Lo, E. C. M. & Yiu, C. K. Y. Combined effect of arginine and fluoride on the growth of *Lactobacillus rhamnosus* GG. *Sci. Rep.* **11** (1), 973. <https://doi.org/10.1038/s41598-020-79684-2> (2021).
75. Li, W. et al. Whole-genome sequencing and genomic-based acid tolerance mechanisms of *Lactobacillus delbrueckii* subsp. *Bulgaricus* LJJ. *Appl. Microbiol. Biotechnol.* **104** (17), 7631–7642. <https://doi.org/10.1007/s00253-020-10788-5> (2020).
76. Prajapati, J. B., Nathani, N. M., Patel, A. K., Senan, S. & Joshi, C. G. Genomic analysis of dairy starter culture *Streptococcus thermophilus* MTCC 5461. *J. Microbiol. Biotechnol.* **23** (4), 459–466. <https://doi.org/10.4014/jmb.1210.10030> (2013).

77. He, Z., Huang, Z., Jiang, W. & Zhou, W. Antimicrobial activity of cinnamaldehyde on *Streptococcus mutans* biofilms. *Front. Microbiol.* **10**, 2241. <https://doi.org/10.3389/fmicb.2019.02241> (2019).
78. Das, M. C. et al. Attenuation of *Pseudomonas aeruginosa* biofilm formation by vitexin: A combinatorial study with azithromycin and gentamicin. *Sci. Rep.* **6**, 23347. <https://doi.org/10.1038/srep23347> (2016).
79. Das, S. et al. Piperine exhibits promising antibiofilm activity against *Staphylococcus aureus* by accumulating reactive oxygen species (ROS). *Arch. Microbiol.* **204** (1), 59. <https://doi.org/10.1007/s00203-021-02642-7> (2021).
80. Otto, M. Staphylococcal biofilms. *Microbiol. Spectr.* **6** (4). <https://doi.org/10.1128/microbiolspec.GPP3-0023-2018> (2018).
81. Das, S. et al. Piperine exhibits potential antibiofilm activity against *Pseudomonas aeruginosa* by accumulating reactive oxygen species, affecting cell surface hydrophobicity and quorum sensing. *Appl. Biochem. Biotechnol.* **195** (5), 3229–3256. <https://doi.org/10.1007/s12010-022-04280-1> (2023).
82. Di Martino, P. Extracellular polymeric substances, a key element in Understanding biofilm phenotype. *AIMS Microbiol.* **4** (2), 274–288. <https://doi.org/10.3934/microbiol.2018.2.274> (2018).
83. Liu, G. et al. Metabolic profiles of carbohydrates in *Streptococcus thermophilus* during pH-controlled batch fermentation. *Front. Microbiol.* **11**, 1131. <https://doi.org/10.3389/fmicb.2020.01131> (2020).
84. Lee, S. M., Hwang, Y. R., Kim, M. S., Chung, M. S. & Kim, Y. S. Comparison of volatile and nonvolatile compounds in rice fermented by different lactic acid bacteria. *Molecules* **24** (6), 1183. <https://doi.org/10.3390/molecules24061183> (2019).
85. Nas, F. et al. A comparative GC-MS analysis of bioactive secondary metabolites produced by halotolerant *Bacillus* spp. Isolated from the great Sebkhah of Oran. *Int. Microbiol.* **24** (3), 455–470. <https://doi.org/10.1007/s10123-021-00185-x> (2021).
86. Halstead, F. D. et al. The antibacterial activity of acetic acid against biofilm-producing pathogens of relevance to burns patients. *PLoS One.* **10** (9), e0136190. <https://doi.org/10.1371/journal.pone.0136190> (2015).
87. Cai, T., Novelli, A., Tascini, C. & Stefani, S. Rediscovering the value of fosfomicin Trometamol in the era of antimicrobial resistance: A systematic review and expert opinion. *Int. J. Antimicrob. Agents* **62** (6), 106983. <https://doi.org/10.1016/j.ijantimicag.2023.106983> (2023).
88. Wang, X. et al. Astemizole as a drug to inhibit the effect of SARS-COV-2 in vitro. *Microb. Pathog.* **156**, 104929. <https://doi.org/10.1016/j.micpath.2021.104929> (2021).
89. Szczerbiec, D., Piechocka, J., Glowacki, R. & Torzewska, A. Organic acids secreted by *Lactobacillus* spp. Isolated from urine and their antimicrobial activity against uropathogenic *Proteus mirabilis*. *Molecules* **27** (17), 5557. <https://doi.org/10.3390/molecules27175557> (2022).
90. Zhao, F., Wang, P., Lucardi, R. D., Su, Z. & Li, S. Natural sources and bioactivities of 2, 4-di-tert-butylphenol and its analogs. *Toxins (Basel)*. **12** (1), 35. <https://doi.org/10.3390/toxins12010035> (2020).
91. Schuster, M., Li, C., Smith, P. & Kuttler, C. Parameters, architecture and emergent properties of the *Pseudomonas aeruginosa* LasI/LasR quorum-sensing circuit. *J. R Soc. Interface.* **20** (200), 20220825. <https://doi.org/10.1098/rsif.2022.0825> (2023).
92. Li, Y. & Ni, M. Regulation of biofilm formation in *Klebsiella pneumoniae*. *Front. Microbiol.* **14**, 1238482. <https://doi.org/10.3389/fmicb.2023.1238482> (2023).
93. Kwon, H. I. et al. Outer membrane protein A contributes to antimicrobial resistance of *Acinetobacter baumannii* through the OmpA-like domain. *J. Antimicrob. Chemother.* **72** (11), 3012–3015. <https://doi.org/10.1093/jac/dkx257> (2017).
94. Conrady, D. G. et al. A zinc-dependent adhesion module is responsible for intercellular adhesion in *Staphylococcal* biofilms. *Proc. Natl. Acad. Sci. U S A.* **105** (49), 19456–19461. <https://doi.org/10.1073/pnas.0807717105> (2008).
95. Magri, M. et al. In Silico identification of natural food compounds as potential quorum-sensing inhibitors targeting the LasR receptor of *Pseudomonas aeruginosa*. *Bioinform Biol. Insights.* **17**, 11779322231212755. <https://doi.org/10.1177/11779322231212755> (2023).
96. Pakharukova, N. et al. Structural basis for *Acinetobacter baumannii* biofilm formation. *Proc. Natl. Acad. Sci. USA.* **115** (21), 5558–5563. <https://doi.org/10.1073/pnas.1800961115> (2018).
97. Huang, Q. et al. The cytoplasmic loops of AgrC contribute to the quorum-sensing activity of *Staphylococcus aureus*. *J. Microbiol.* **59** (1), 92–100. <https://doi.org/10.1007/s12275-021-0274-x> (2021).
98. Chao, P. et al. Integration of molecular Docking and molecular dynamics simulations with subtractive proteomics approach to identify the novel drug targets and their inhibitors in *Streptococcus galloyticus*. *Sci. Rep.* **14**, 14755. <https://doi.org/10.1038/s41598-024-64769-z> (2024).
99. Chio, H. et al. Predicting bioactivity of antibiotic metabolites by molecular Docking and dynamics. *J. Mol. Graph. Model.* **123**, 108508. <https://doi.org/10.1016/j.jmgm.2023.108508> (2023).
100. Ibraheim, M. H., Maher, I. & Khater, I. In Silico repurposing of a novel inhibitor (drug) of EGFR and VEGFR-2 kinases of cancer by pharmacokinetics, toxicity, molecular docking, and molecular dynamics simulation. *Appl. Biochem. Biotechnol.* <https://doi.org/10.1007/s12010-024-04958-8> (2024).

## Acknowledgements

Authors are thankful to support Biokart India Pvt. Ltd. Bengaluru, Karnataka 560043, India for whole genome sequencing service.

## Author contributions

A.S. and I.K.N. wrote Methodology, D.D., G.G., and Z.T. performed formal analysis and investigation; and I.C. wrote original draft, review and editing, supervision and funding acquisition. All authors read and approved the final manuscript.

## Funding

This work was supported by Indian Council of Medical Research, New Delhi (45/2020–2541/Gen/Adhoc-BMS & 5/4/2–8/OH/2022-NCD-II). Author A.S. has received research support from UGC-SRF fellowship (865/CSIR-UGC NET DEC-2018) and Author Z.T. has received research support from Indian Council of Medical Research, New Delhi (ICMR-RA/3/1/2(3)/OH/2022-NCD-II).

## Declarations

## Competing interests

The authors declare no competing interests.

## Additional information

**Supplementary Information** The online version contains supplementary material available at <https://doi.org/1>

[0.1038/s41598-025-90999-w](https://doi.org/10.1038/s41598-025-90999-w).

**Correspondence** and requests for materials should be addressed to I.C.

**Reprints and permissions information** is available at [www.nature.com/reprints](http://www.nature.com/reprints).

**Publisher's note** Springer Nature remains neutral with regard to jurisdictional claims in published maps and institutional affiliations.

**Open Access** This article is licensed under a Creative Commons Attribution-NonCommercial-NoDerivatives 4.0 International License, which permits any non-commercial use, sharing, distribution and reproduction in any medium or format, as long as you give appropriate credit to the original author(s) and the source, provide a link to the Creative Commons licence, and indicate if you modified the licensed material. You do not have permission under this licence to share adapted material derived from this article or parts of it. The images or other third party material in this article are included in the article's Creative Commons licence, unless indicated otherwise in a credit line to the material. If material is not included in the article's Creative Commons licence and your intended use is not permitted by statutory regulation or exceeds the permitted use, you will need to obtain permission directly from the copyright holder. To view a copy of this licence, visit <http://creativecommons.org/licenses/by-nc-nd/4.0/>.

© The Author(s) 2025